On the solution to the Riemann problem for the compressible duct flow

Nikolai Andrianov and Gerald Warnecke*

March 6, 2003

Abstract

The quasi-one-dimensional Euler equations in a duct of variable cross-section are probably one of the most simplest non-conservative systems. We consider the Riemann problem for it and discuss its properties. In particular, for some initial conditions, the solution to the Riemann problem appears to be non-unique. In order to rule out the non-physical solutions, we provide 2D computations of the Euler equations in a duct of corresponding geometry and compare it with the 1D results. Then, the physically relevant 1D solutions satisfy a kind of entropy rate admissibility criterion. Finally, we present a procedure for finding an exact solution to the Riemann problem and construct a Godunov-type method on its basis.

Keywords. Nozzle flow, nonstrictly hyperbolic, resonance, Godunov method
2000 Mathematics Subject Classification. 35L65, 35L67, 76N99

1 Introduction

In the past decades, a considerable attention has been paid to both theoretical and numerical investigations of systems of conservation laws. This interest is caused by a wide range of applications of conservation laws, like fluid mechanics, astrophysics, meteorology etc. However, there is an important class of problems which is described by the *non-conservative* systems, i.e. systems, which cannot be written in divergence form. The example which we will have in mind is two-phase flows.

The theory of non-conservative systems is still under development. The same can be said about the numerical methods for such systems. Here, we consider

*IAN, Otto-von-Guericke Universität Magdeburg, PSF 4120, D-39016 Magdeburg, Germany. Email: {nikolai.andrianov | gerald.warnecke}@mathematik.uni-magdeburg.de

probably one of the most simple non-conservative systems, the system of the Euler equations in a duct of variable cross-section. In our previous work [3] we have shown that this system can be formally obtained from the Baer–Nunziato model of two-phase flows [6], which describes the flame spread and the deflagration-to-detonation transition (DDT) in gas-permeable, reactive granular materials. Therefore, the results of [3] to a certain extent will also hold for the Euler equations in a duct of variable cross-section. Conversely, a number of results which we present here are also valid for the Baer–Nunziato model in [3].

One can distinguish two parts in the system of the Euler equations in a duct. These are a strictly hyperbolic system and an additional equation, which states that the cross-section does not change in time. The resulting system appears to be only non-strictly hyperbolic with the *resonant behaviour*, when one of the nonlinear wave families has a zero wave speed. Such resonant systems have been studied before, see Isaacson and Temple [16, 17] and the references therein. We refer also to a recent work of Goatin and LeFloch [14] for a study of the Riemann problem for non-conservative resonant systems.

There are several difficulties concerning the solution of non-conservative systems. Due to the presence of non-conservative terms one cannot use the definition of a weak solution from the theory of conservation laws. A general definition based on the theory of non-conservative products was given in Dal Maso, LeFloch, and Murat [12]. For the particular case of the Riemann problem to the Euler equations in a duct, it appears that the system of governing equations is locally equivalent to some conservative system. This allows us to give a corresponding definition of weak solution, see Section 3.

It appears that for certain initial conditions, the solution to the Riemann problem is not unique, despite the fact that all shocks satisfy locally a usual entropy criterion. We discuss the conditions which lead to non-uniqueness. For the selection of a physically relevant solution we compare some examples with 2D duct flow computations. The 1D solutions picked out by 2D computations satisfy a kind of entropy rate admissibility criterion in analogy to Dafermos [10].

Finally, it is not clear how to discretize non-conservative systems in order to obtain an adequate numerical method. Indeed, the foundation-stone of the numerical methods for conservation laws is the *conservation principle*. Obviously, it does not hold for non-conservative systems. However, for the Euler equations in a duct, the non-conservative terms act only along one *stationary* wave in the solution of local Riemann problems at cell boundaries. This is a key observation for constructing a Godunov-type method for this system, see Section 7.

The paper is organized as follows. In Section 2 we carry out the characteristic analysis of the system of governing equations. In Section 3 we introduce the notion of a weak solution for the Riemann problem. Section 6 is devoted to finding of an exact solution to the Riemann problem. Finally, in Section 7 we present a Godunov-type method for the numerical solution of the Euler equations in a duct of variable cross-section.

2 Mathematical analysis

The system of the Euler equations in a duct of variable cross section is usually written in the following form

$$\begin{aligned} \frac{\partial A\rho}{\partial t} + \frac{\partial A\rho v}{\partial x} &= 0 \\ \frac{\partial A\rho v}{\partial t} + \frac{\partial A(\rho v^2 + p)}{\partial x} &= p\frac{\partial A}{\partial x} \\ \frac{\partial A\rho E}{\partial t} + \frac{\partial Av(\rho E + p)}{\partial x} &= 0. \end{aligned} \tag{2.1}$$

For the derivation, see e.g. Zucrow and Hoffman [27]. Here, $A = A(x)$ is the variable cross-section, ρ is the density, v the velocity, p the pressure, $E = e + v^2/2$ the specific total energy. We assume that the gas obeys the stiffened gas equation of state (EOS),

$$e = \frac{p + \gamma\pi}{\rho(\gamma - 1)}, \tag{2.2}$$

where γ, π are the thermodynamic constants. When $\pi = 0$ we recover the usual ideal gas EOS. To close the system (2.1), we need another condition on $A = A(x)$. Usually, the cross-section $A = A(x)$ is assumed to be given *a priori*. However, we can consider it as an additional unknown, and supply the trivial equation $A_t = 0$ for determining it. Then the system (2.1) becomes

$$\mathbf{u}_t + \mathbf{f}(\mathbf{u})_x = \mathbf{H}(\mathbf{u})\, A_x, \tag{2.3}$$

where

$$\mathbf{u} = \begin{bmatrix} A \\ A\rho \\ A\rho v \\ A\rho E \end{bmatrix}, \qquad \mathbf{f}(\mathbf{u}) = \begin{bmatrix} 0 \\ A\rho v \\ A(\rho v^2 + p) \\ Av(\rho E + p) \end{bmatrix}, \qquad \mathbf{H}(\mathbf{u}) = \begin{bmatrix} 0 \\ 0 \\ p \\ 0 \end{bmatrix}. \tag{2.4}$$

In what follows, we will often consider the Riemann problem for (2.3), i.e. equip it with piecewise constant initial data

$$\mathbf{u}(x, 0) = \begin{cases} \mathbf{u}_L, & x \le x_0 \\ \mathbf{u}_R, & x > x_0. \end{cases} \tag{2.5}$$

As we have noted in [3], the system (2.3) can be formally obtained from the governing equations for the Baer–Nunziato model of two-phase flows [6]. Therefore the analysis of (2.3) appears to be very similar to that of [3]. A particular issue about the system (2.3) is the presence of the *non-conservative term* $p\,\partial A/\partial x$ in the system (2.3). Due to this term, we cannot write (2.3) in divergence form. Consequently, we cannot define a weak solution and find the

Rankine–Hugoniot conditions in the usual way, as it is done for the systems of conservation laws.

To carry out the characteristic analysis of (2.3), it is convenient to use the primitive variables

$$\mathbf{v} = (A, \rho, v, p)^T. \tag{2.6}$$

Then, for smooth solutions, the system (2.3) is equivalent to

$$\mathbf{v}_t + \mathbf{A}(\mathbf{v})\mathbf{v}_x = 0, \tag{2.7}$$

where

$$\mathbf{A} = \begin{bmatrix} 0 & 0 & 0 & 0 \\ \rho v/A & v & \rho & 0 \\ 0 & 0 & v & 1/\rho \\ \rho v c^2/A & 0 & \rho c^2 & v \end{bmatrix}, \tag{2.8}$$

and $c = \sqrt{\gamma(p+\pi)/\rho}$ is the sound speed. The eigenvalues of $\mathbf{A}$ are

$$\lambda_0 = 0, \quad \lambda_1 = v - c, \quad \lambda_2 = v, \quad \lambda_3 = v + c, \tag{2.9}$$

and the corresponding eigenvectors are

$$\mathbf{r}_0 = \begin{bmatrix} A(v^2 - c^2)/c^2 \\ -v^2\rho/c^2 \\ v \\ -\rho v^2 \end{bmatrix}, \ \mathbf{r}_1 = \begin{bmatrix} 0 \\ -\rho \\ c \\ -\rho c^2 \end{bmatrix}, \ \mathbf{r}_2 = \begin{bmatrix} 0 \\ 1 \\ 0 \\ 0 \end{bmatrix}, \ \mathbf{r}_3 = \begin{bmatrix} 0 \\ \rho \\ c \\ \rho c^2 \end{bmatrix}. \tag{2.10}$$

Note that the situations are possible, when either of λ_1, λ_2, or λ_3 coincides with λ_0. Moreover, when λ_1 or λ_3 coincide with λ_0, the corresponding eigenvectors become linearly dependent. In this case a parabolic degeneracy occurs. To summarize, the system of governing equations (2.3) is non-strictly hyperbolic away from the points where either $\lambda_1 = \lambda_0$ or $\lambda_3 = \lambda_0$.

We can easily establish that the first three characteristic fields are exactly the same as for the usual one-dimensional Euler equations. The first and third characteristic fields are genuinely nonlinear, and the second is linearly degenerate. It is obvious that the 0-characteristic field is also linearly degenerate.

The Riemann initial data for (2.7) are

$$\mathbf{v}(x, 0) = \begin{cases} \mathbf{v}_L, & x \le x_0 \\ \mathbf{v}_R, & x > x_0. \end{cases} \tag{2.11}$$

It is well known that the Riemann problem (2.7), (2.11) admits self-similar solutions, i.e.

$$\mathbf{v}(x, t) = \mathbf{v}(\xi), \qquad \xi = \frac{x - x_0}{t}. \tag{2.12}$$

If we use the equation by state of the form (2.2), then the solution of the Riemann problem (2.3), (2.11) can consist of shock waves, contact discontinuities, or rarefaction waves. It is easy to establish that the Riemann invariants for first three fields coincide with those of the Euler equations. Also, the cross-section A is constant across them. The Riemann invariants across the 0-contact are

$$\begin{aligned} A\rho v &= \text{const} \\ \eta &= \text{const} \\ \frac{v^2}{2} + \frac{c^2}{\gamma - 1} &= \text{const}, \end{aligned} \tag{2.13}$$

where $\eta = (p + \pi)/\rho^\gamma$ is the isentrope. Note that the relations (2.13) express the conservation of mass, entropy, and Bernoulli's law, respectively, see e.g. Courant and Friedrichs [9].

There exist at most two solutions to the system (2.13), see [3]. We determine which solution will be admissible using the criterion of [3]. It states that the eigenvalues on the both sides of the 0-contact do not change their sign. Then the 0-contact will be an *evolutionary* discontinuity, i.e. it will remain in the solution to (2.3), (2.5). Further, one can then show that the corresponding 0-wave curve will be admissible in sense of Isaacson and Temple [16], see also Goatin and LeFloch [14].

3 Weak solution to the Riemann problem

One of the mathematical difficulties which appears when one works with non-conservative systems is that one cannot define a weak solution in the usual manner, as it is done for systems of conservation laws. However, for the particular case of the Riemann problem (2.3), (2.5) the non-conservative term $p\,\partial A/\partial x$ plays a role only across one wave in the solution, the stationary 0-contact. In the rest of domain, A is constant and equal to its left or right value,

$$A(x) = \begin{cases} A_L, & x \text{ lies to the left of stationary contact} \\ A_R, & x \text{ lies to the right of it.} \end{cases}$$

Therefore, everywhere away from the stationary contact the system (2.3) reduces to the usual one-dimensional Euler equations

$$\mathbf{u}_t + \mathbf{f}(\mathbf{u})_x = 0, \tag{3.1}$$

where

$$\mathbf{u} = \begin{bmatrix} \rho \\ \rho v \\ \rho E \end{bmatrix}, \quad \mathbf{f}(\mathbf{u}) = \begin{bmatrix} \rho v \\ \rho v^2 + p \\ v(\rho E + p) \end{bmatrix}. \tag{3.2}$$

For the system (3.1), we can define a weak solution in the usual manner.

On the other hand, across the stationary contact, the relations (2.13) hold. Our main idea is to find a system of equations, which give the relations (2.13)

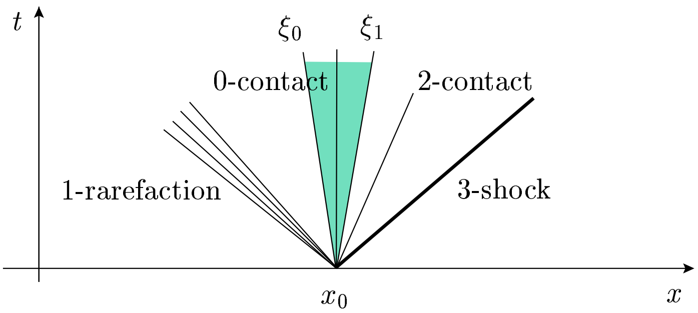

Fig. 1. A typical Riemann problem for the one-dimensional Euler equations in a duct.

across the stationary contact. In other words, we reverse the usual process of obtaining the Rankine–Hugoniot conditions for a system of conservation laws. There, one starts with the system of equations and gets the relations across a discontinuity. Here, we start from the relations across the discontinuity and wish to find the system of equations.

Across the stationary contact the flow is isentropic, see (2.13). As long as some other waves do not coincide with the stationary contact, we can choose a small sector around the stationary contact where the flow is isentropic, too. Consider Fig. 1 for a typical Riemann problem. The solution in the sector, bounded by the rays ξ_0 and ξ_1 around the stationary contact, is governed by the relations (2.13). In the left and in the right parts of this sector, the system (2.3) is equivalent to the system

$$\begin{aligned} \frac{\partial A}{\partial t} &= 0 \\ \frac{\partial A\rho}{\partial t} + \frac{\partial A\rho v}{\partial x} &= 0 \\ \frac{\partial A\rho E}{\partial t} + \frac{\partial Av(\rho E + p)}{\partial x} &= 0 \\ \frac{\partial \eta}{\partial t} + v\frac{\partial \eta}{\partial x} &= 0. \end{aligned} \tag{3.3}$$

Note that the last equation in (3.3) is trivially satisfied everywhere in the sector, since the flow is isentropic there. Therefore, the system (3.3) may be rewritten as

$$\mathbf{U}_t + \mathbf{F}(\mathbf{U})_x = 0, \tag{3.4}$$

where

$$\mathbf{U} = \begin{bmatrix} A \\ A\rho \\ A\rho E \end{bmatrix}, \quad \mathbf{F}(\mathbf{U}) = \begin{bmatrix} 0 \\ A\rho v \\ Av(\rho E + p) \end{bmatrix}. \tag{3.5}$$

The Rankine–Hugoniot conditions for this system, augmented with the condition $\eta = \text{const}$, coincide with the relations (2.13). Since the system (3.4) is in divergence form now, we can use the usual definition of a weak solution for it. Note that the approach we have used here is exactly the same as that of [3].

Consider a system of conservation laws

$$\mathbf{u}_t + \mathbf{f}(\mathbf{u})_x = 0, \tag{3.6}$$

where the pair $(\mathbf{u}, \mathbf{f}(\mathbf{u}))$ are either $(\mathbf{u}, \mathbf{f}(\mathbf{u}))$ in (3.2) or $(\mathbf{U}, \mathbf{F}(\mathbf{U}))$ in (3.5), and let us restrict ourselves to self-similar solutions of it. Then, for the smooth solutions, this system is equivalent to

$$-\mathbf{v}_\xi \cdot \xi + \mathbf{f}(\mathbf{v})_\xi = 0. \tag{3.7}$$

Consider the Riemann problem for it, i.e. augment (3.7) with constant initial data

$$\mathbf{v}(-\infty) = \mathbf{v}_L, \quad \mathbf{v}(\infty) = \mathbf{v}_R. \tag{3.8}$$

If we multiply (3.7) by a test function $\phi \in C_0^1(]\xi_0, \xi_1[)$ and integrate over all ξ, we get

$$\int_{\xi_0}^{\xi_1} (\mathbf{v}(\phi \cdot \xi)_\xi - \mathbf{f}(\mathbf{v})\phi_\xi)\, d\xi = 0. \tag{3.9}$$

Now $\mathbf{v}$ does not need to be differentiable anymore, and we can use it to define a weak solution to the Riemann problem (3.7), (3.8). Remember, that *locally* the *non-conservative* system (2.3) can be reduced to a conservative one, either (3.1) or (3.4). Thus, now we can give a definition of a *global* weak solution to the Riemann problem (2.3), (2.5) as a composition of the weak solutions to the conservative systems (3.1) and (3.4).

Definition 3.1. *Consider a sector*

$$S(\xi_0, \xi_1) = \{(x,t) \in \mathbb{R} \ : \ \xi_0 \leq \frac{x}{t} \leq \xi_1\},$$

*bounded by the rays ξ_0 and ξ_1, such that the stationary contact lies in it, and assume that it is the only ray of discontinuity there. Then, a function $\mathbf{v} = \mathbf{v}(\xi) \in L^\infty_{loc}(\mathbb{R})$ is called a **weak solution of the Riemann problem** (2.3), (2.5), if for any small $\epsilon > 0$*

1. *To the left of ξ_0, i.e., $\xi \in]-\infty, \xi_0]$,*

$$\int_{-\infty}^{\xi_0} (\mathbf{v}(\phi \cdot \xi)_\xi - \mathbf{f}(\mathbf{v})\phi_\xi)\, d\xi = 0, \qquad \textit{for all} \ \ \phi \in C_0^1(]-\infty, \xi_0 + \epsilon[),$$

$\mathbf{v}(\xi) = \mathbf{u}(x,t)$, $\mathbf{f}(\mathbf{v}) = \mathbf{f}(\mathbf{u})$, *and* $\mathbf{u}$, $\mathbf{f}(\mathbf{u})$ *are given by* (3.2).

2. *To the right of* ξ_1*, i.e.,* $\xi \in [\xi_1, \infty[$*,*

$$\int_{\xi_1}^{\infty} (\mathsf{v}(\phi \cdot \xi)_\xi - \mathsf{f}(\mathsf{v})\phi_\xi)\, d\xi = 0, \qquad \text{for all} \;\; \phi \in C_0^1(]\xi_1 - \epsilon, \infty[),$$

$\mathsf{v}(\xi) = \mathbf{u}(x,t)$*,* $\mathsf{f}(\mathsf{v}) = \mathbf{f}(\mathbf{u})$*, and* $\mathbf{u}$*,* $\mathbf{f}(\mathbf{u})$ *are given by* (3.2)*.*

3. *Inside of the sector, bounded by* ξ_0 *and* ξ_1*, i.e.,* $\xi \in [\xi_0, \xi_1]$*,*

$$\int_{\xi_0}^{\xi_1} (\mathsf{v}(\phi \cdot \xi)_\xi - \mathsf{f}(\mathsf{v})\phi_\xi)\, d\xi = 0, \qquad \text{for all} \;\; \phi \in C_0^1(]\xi_0 - \epsilon, \xi_1 + \epsilon[),$$

$\mathsf{v}(\xi) = \mathbf{U}(x,t)$*,* $\mathsf{f}(\mathsf{v}) = \mathbf{F}(\mathbf{U})$*, and* $\mathbf{U}$*,* $\mathbf{F}(\mathbf{U})$ *are given by* (3.5)*.*

Remark 1. Note that in the sector $S(\xi_0 - \epsilon, \xi_0 + \epsilon)$, the definitions 1) and 3) coincide, and in the sector $S(\xi_1 - \epsilon, \xi_1 + \epsilon)$, the definitions 2) and 3) coincide.

Remark 2. In [12], Dal Maso, LeFloch, and Murat introduce a notion of the non-conservative product and give a definition of a weak solution to a general non-conservative system on its basis. In particular, this applies also to the system (2.3). In contrast to the definition of [12], we have used some physical observations in Definition 3.1, which are valid only for systems of a certain structure like (2.3), or the Baer–Nunziato model we considered in [3]. Therefore, it might be helpful in choosing a criterion for a physically admissible solution to the Riemann problem for such systems. This question becomes especially important since the solution to the Riemann problem (2.3), (2.5) is in general not unique, see Section 4.

4 Non-uniqueness of the Riemann solution

It appears that the solution to the Riemann problem (2.3), (2.5) is in general non-unique. For the same left and right states $\mathbf{u}_L, \mathbf{u}_R$, one can get completely different Riemann solutions. The reason for this behaviour is that the system (2.3) is *non-strictly* hyperbolic. For the Riemann problem (2.3), (2.5) it means that the mutual position of the waves, configuration of the Riemann problem, can change, see Fig. 2 for the four possible cases. As soon as we fix the configuration, the solution to the Riemann problem is unique. The problem of non-uniqueness arises from the fact that for certain sets of initial data more than one configuration is possible. In this light it makes sense to consider the conditions, which lead to the different configurations of the Riemann problem.

In what follows, we will make extensive use of the wave curves for the Riemann problem (2.3), (2.5). These are the curves in the (v,p)-plane which represent the states which can be connected to $\mathbf{u}_L, \mathbf{u}_R$ by the admissible waves. The shock and rarefaction wave curves will be given by formula (6.6). It can be shown that the 1-curve, shock or rarefaction, is strictly increasing, and the 3-curve is strictly

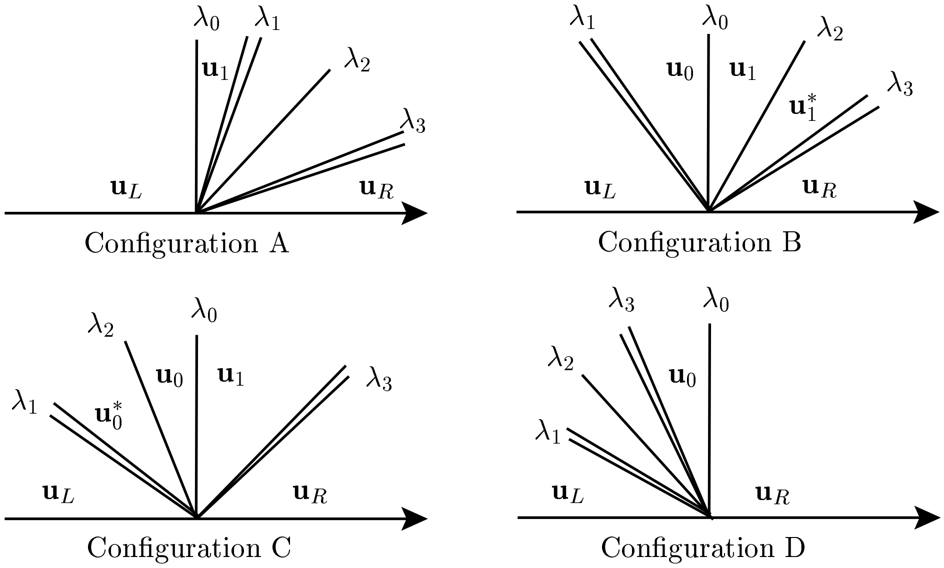

Fig. 2. Possible configurations of the Riemann problem.

decreasing, see e.g. Godlewski and Raviart [15]. Further, the left and right states of the 2-wave are projected to the same point in the (v, p)-plane. Therefore, the Riemann problem for the usual Euler equations (2.3), (2.5) with $A_L = A_R$ has a unique solution, see e.g. [15, Theorem 3.1, p. 134].

In the solution of the Riemann problem with $A_L \neq A_R$, a jump appears across the stationary contact λ_0, i.e., there is a new wave in the solution of the Riemann problem. In what follows, we will call this wave the *0-wave*. In [3], we have shown that the flow inside this wave is analogous to the stationary isentropic flow in the converging-diverging nozzle. For convenience, we repeat the main consequences of this fact here:

- The stationary contact can be viewed as a porous film of infinitesimal thickness
- Each pore is a converging-diverging nozzle; the cross-sections on each side of it are A_L and A_R, respectively
- The velocity inside a pore does not change its sign; moreover, if the flow is sub(super)sonic at the inlet, it is also sub(super)sonic at the outlet
- The change of the flow parameters in a pore is given by the following table, where $\uparrow$ stands for increasing and $\downarrow$ for decreasing:

Supersonic	$A\uparrow$	$v\uparrow$	$p\downarrow$	$c\downarrow$	$\rho\downarrow$
	$A\downarrow$	$v\downarrow$	$p\uparrow$	$c\uparrow$	$\rho\uparrow$
Subsonic	$A\uparrow$	$v\downarrow$	$p\uparrow$	$c\uparrow$	$\rho\uparrow$
	$A\downarrow$	$v\uparrow$	$p\downarrow$	$c\downarrow$	$\rho\downarrow$

For a given left state $\mathbf{u}_0$ of the stationary contact we can represent the 0-wave curve parametrically by A as follows,

$$\begin{cases} \rho = \rho(A; \mathbf{u}_0) \\ v = v(A; \mathbf{u}_0) \\ p = p(A; \mathbf{u}_0), \end{cases} \tag{4.1}$$

where the states must satisfy (2.13). The three-dimensional curve (4.1) will be regular if the corresponding derivatives are continuous, therefore locally bounded, and are non-zero simultaneously, i.e. the tangent vector does not vanish,

$$\left(\frac{\partial \rho}{\partial A}, \frac{\partial v}{\partial A}, \frac{\partial p}{\partial A}\right) \neq 0. \tag{4.2}$$

We will formulate the following lemma under these conditions; later on, we will discuss situations when they are violated.

Lemma 4.1. *Consider the Riemann problem* (2.3), (2.5) *with the stiffened gas EOS* (2.2)*, and denote the states connected by the 0-wave by* $\mathbf{u}_0$ *and* $\mathbf{u}_1$*. Assume that the conditions* (4.2) *are fulfilled. The flow velocity v inside the 0-wave does not change its sign, and is either subsonic, or supersonic everywhere in the flow. Denote its* ***signed Mach number*** *by* $\mathrm{M} = \frac{v}{c}$*. Then for the 0-wave curve* (4.1) *the following statements are true*

1. *The 0-wave curve is strictly increasing(decreasing) in p, if $v < 0 (> 0)$.*

2. *The 0-wave curve is convex(concave) with respect to p, if $|\mathrm{M}| > 1 (< 1)$.*

3. *For increasing(decreasing) velocities and pressures in $\mathbf{u}_0$, the velocities and pressures in $\mathbf{u}_1$ also increase(decrease) and vice versa.*

4. *For the states $\mathbf{u}_0$ and $\mathbf{u}_1$,*

$$\begin{cases} \rho_0 \to \bar{\rho} \\ v_0 \to 0 \\ p_0 \to \bar{p} \end{cases} \iff \begin{cases} \rho_1 \to \bar{\rho} \\ v_1 \to 0 \\ p_1 \to \bar{p} \end{cases}$$

for all $\bar{\rho}, \bar{p} > 0$.

Proof. We take (4.1) and fix $\mathbf{u}_0$, so that ρ, v and p only depend on A. Since the flow inside the 0-wave is analogous to the converging-diverging flow, see [3], we take the following relations from Courant and Friedrichs [9, (145.05), (145.08)], i.e.

$$\frac{dA}{A} + \frac{d\rho}{\rho} + \frac{dv}{v} = 0 \tag{4.3}$$

$$\frac{dA}{A} = \left(\frac{v^2}{c^2} - 1\right)\frac{dv}{v}, \tag{4.4}$$

where A is the variable cross-section of a pore (see above), ρ, c, and v are the corresponding parameters of the flow in the pore. Then (4.4) leads to

$$\frac{dv}{dA} = \frac{vc^2}{A(v^2 - c^2)}. \tag{4.5}$$

By the definition of the sound speed

$$\left.\frac{dp}{d\rho}\right|_{\eta} = c^2, \qquad \text{i.e.} \qquad \frac{d\rho}{\rho} = \frac{dp}{\rho c^2}.$$

Substituting this into (4.3), we obtain

$$\frac{dp}{dA} = \rho c^2 \left(-\frac{1}{A} - \frac{1}{v}\frac{dv}{dA}\right) = -\frac{\rho v^2 c^2}{A(v^2 - c^2)}. \tag{4.6}$$

Analogously,

$$\frac{d\rho}{dA} = -\frac{\rho v^2}{A(v^2 - c^2)}. \tag{4.7}$$

Now we see when the 0-wave curve will be regular, i.e. the conditions (4.2) will be fulfilled. From (4.5), (4.6), and (4.7) it follows that this will happen when either

$$v \neq 0 \qquad \text{or} \qquad |v| \neq c. \tag{4.8}$$

From now on, when discussing 0-wave curves, we will always assume that the conditions (4.8) are fulfilled, unless stated otherwise.

Consider the system of ordinary differential equations (4.5), (4.6), (4.7)

$$\frac{d}{dA}\begin{pmatrix} \rho \\ v \\ p \end{pmatrix} = \frac{1}{A(v^2 - c^2)}\begin{pmatrix} -\rho v^2 \\ vc^2 \\ -\rho v^2 c^2 \end{pmatrix} \tag{4.9}$$

with the initial data

$$\begin{cases} \rho(A_0) &= \rho_0 \\ v(A_0) &= v_0 \\ p(A_0) &= p_0 \end{cases}$$

A straightforward calculation shows that under conditions (4.8), the functions on the right-hand side of (4.9) are differentiable for $A > 0$. Then by the existence

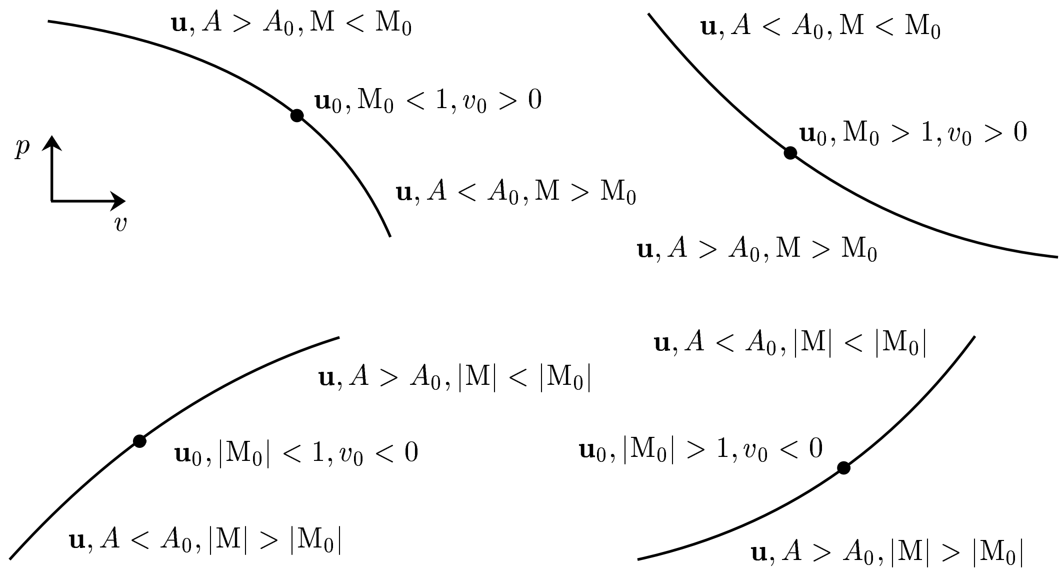

Fig. 3. The 0-curves in the (v, p)-plane, parametrized with A, connect the states $\mathbf{u}_0$ and $\mathbf{u}$. Depending on v_0, M_0, the curves exhibit different behaviour.

and uniqueness theorem there exists a unique integral curve of (4.9) as long as the right-hand side is Lipschitz continuous. This curve is nothing else but the 0-wave curve, passing through the point $\mathbf{u}_0$. Note that all states with $v = 0$ are stationary points of the system (4.9). Therefore, the solutions may approach such states only asymptotically.

From (4.5) and (4.6), we obtain

$$\frac{dp}{dv} = -\rho v$$

and thus the statement 1 is proved. Of course, it can be also seen from the table above.

For the proof of the statement 2, we calculate using (4.5) and (4.6)

$$\frac{d^2p}{dv^2} = -\frac{d\rho}{dv}v - \rho = \rho\left(\frac{v^2}{c^2} - 1\right),$$

which gives the desired result. The possible 0-waves are presented in Fig. 3.

Using $\eta = \frac{p+\pi}{\rho^\gamma}$ in the relations (2.13) across the 0-wave, we get

$$v_1 = v_0\frac{A_0}{A_1}\left(\frac{p_0}{p_1}\right)^{1/\gamma}$$
$$p_1 = p_0\left(\frac{A_0 v_0}{A_1 v_1}\right)^{\gamma}.$$

Note that v_0 and v_1 always have the same sign, cf. (2.13). Differentiating the above equations with respect to v_0 and p_0 respectively, we get

$$\begin{aligned}\frac{\partial v_1}{\partial v_0} &= \frac{A_0}{A_1}\left(\frac{p_0}{p_1}\right)^{1/\gamma} > 0 \\ \frac{\partial p_1}{\partial p_0} &= \left(\frac{A_0 v_0}{A_1 v_1}\right)^{\gamma} > 0,\end{aligned}$$

thus proving the statement 3.

For the statement 4, it is enough to prove only "$\Longrightarrow$", since the statement is symmetric with respect to subscripts 0 and 1. Using $\eta = \frac{p+\pi}{\rho^\gamma}$ and $c^2 = \frac{\gamma(p+\pi)}{\rho}$ in the relations (2.13), we obtain

$$A_0(p_0+\pi)^{1/\gamma}v_0 = A_1(p_1+\pi)^{1/\gamma}v_1 \tag{4.10}$$

$$\frac{p_0+\pi}{\rho_0^\gamma} = \frac{p_1+\pi}{\rho_1^\gamma} \tag{4.11}$$

$$\frac{v_0^2}{2} + \frac{\gamma\eta^{1/\gamma}(p_0+\pi)^{1-1/\gamma}}{\gamma-1} = \frac{v_1^2}{2} + \frac{\gamma\eta^{1/\gamma}(p_1+\pi)^{1-1/\gamma}}{\gamma-1}. \tag{4.12}$$

We wish to show that p_1 remains bounded, i.e. $p_1 \not\to \infty$. Then by statement 1 the pressure p_1 must exceed p_0, $p_1 > p_0$. Using that the left-hand side of (4.12) is bounded, the estimate

$$\frac{v_1^2}{2} + \frac{\gamma\eta^{1/\gamma}(p_1+\pi)^{1-1/\gamma}}{\gamma-1} > \frac{\gamma\eta^{1/\gamma}(p_1+\pi)^{1-1/\gamma}}{\gamma-1}$$

will give us the desired result that $p_1 <$ const, since γ, $\pi > 0$ are constants, and η is constant along the 0-curve.

Now the equation (4.10) implies that $v_1 \to 0$. Using this in (4.12), we get $p_1 \to \bar{p}$. Finally, by (4.11) is also $\rho_1 \to \bar{\rho}$, which proves the statement 4.

□

Let us represent in the (v, p)-plane the possible scenarios of the solution of the Riemann problem (2.3), (2.5), which can lead to a solution in the form of the configuration B, see Fig. 2. For this configuration, the 0-wave is next to the 1-wave. In the (v, p)-plane it means that the possible 0-curves necessarily start from the 1-wave curve. The correct 0-wave curve, i.e. the one which gives the solution to the Riemann problem (2.3), (2.5), connects the 1- and 3-curves in the (v, p)-plane. Figs. 4, 5 represent the wave curves for the configuration B.

Denote the states, connected by the 0-curve, by $\mathbf{u}_0$ and $\mathbf{u}_1$, and let $\mathbf{u}_0$ lie on the 1-curve. Observe that not all states $\mathbf{u}_0$ come into consideration. Indeed, by definition of configuration B, the velocities in the states $\mathbf{u}_0$ and $\mathbf{u}_1$ must be non-negative. In configuration B the 1-wave has a non-positive velocity and therefore the right-hand velocity $v_0 - c_0$ of its characteristic family must also be

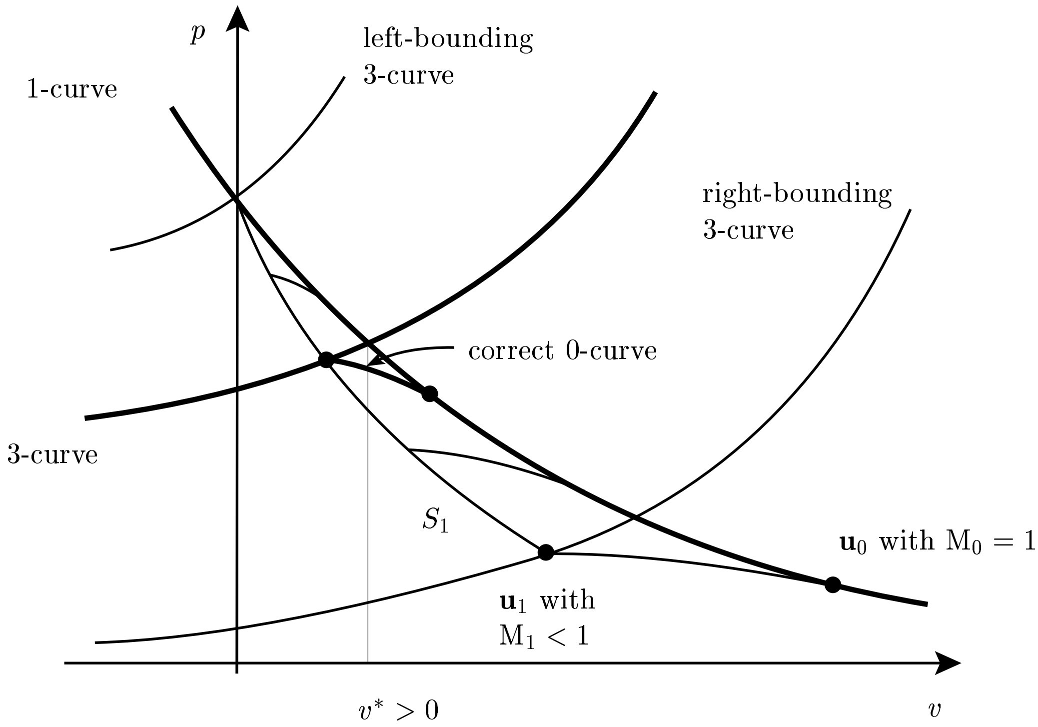

Fig. 4. The wave curves for the configuration B with $A_L < A_R$.

non-positive, $v_0 - c_0 \leq 0$. In terms of the Mach number, it means that $\mathrm{M}_0 \leq 1$. Therefore, the candidates for $\mathbf{u}_0$ have necessarily $0 \leq \mathrm{M}_0 \leq 1$. This gives rise to the following definition.

Definition 4.2. *Consider the Riemann problem* (2.3), (2.5). *Let us call the 3-curve, crossing the 1-curve in the point with* $v = 0$ *the* ***left-bounding 3-curve****. Further,*

1. *If* $A_L < A_R$*, consider the state* $\mathbf{u}_0$ *on the 1-curve with* $\mathrm{M}_0 = 1$*, connected with the state* $\mathbf{u}_1$ *with* $\mathrm{M}_1 < 1$ *by the 0-wave. Let us call the 3-curve passing through* $\mathbf{u}_1$ *the* ***right-bounding 3-curve****, see Fig. 4.*

2. *If* $A_L > A_R$*, consider the state* $\mathbf{u}_0$ *on the 1-curve with* $\mathrm{M}_0 < 1$*, connected with the state* $\mathbf{u}_1$ *with* $\mathrm{M}_1 = 1$ *by the 0-wave. Let us call the 3-wave, passing through this state* $\mathbf{u}_1$*, the* ***right-bounding 3-curve****, see Fig. 5.*

Remark 3. We cannot use the results of Lemma 4.1 in Definition 4.2, since the parametrization (4.1) of the 0-wave will be singular for $\mathrm{M} = 1$, cf. (4.8). However, taking v as the 0-curve parameter in a neighborhood of sonic points,

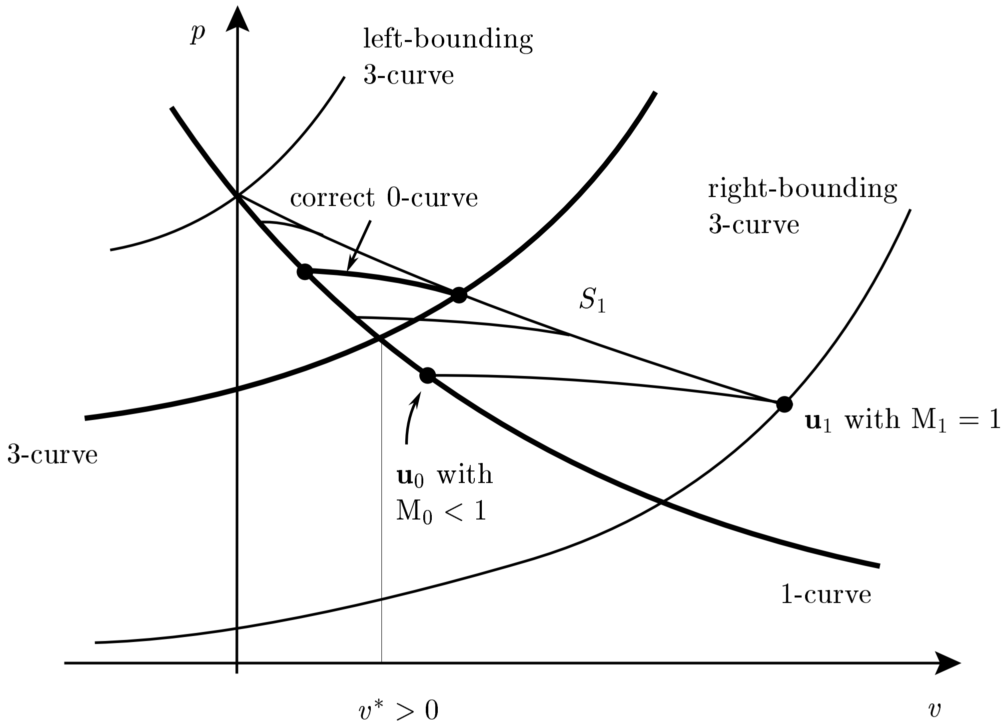

Fig. 5. The wave curves for the configuration B with $A_L > A_R$.

i.e. replacing (4.9) by the system

$$\frac{d}{dv}\begin{pmatrix} A \\ \rho \\ p \end{pmatrix} = \begin{pmatrix} A/v \cdot (v^2 - c^2)/c^2 \\ -\rho v/c^2 \\ -\rho v \end{pmatrix},$$

one can show that the length of the 0-wave curve remains finite.

Now we are ready to establish when the solution to the Riemann problem (2.3), (2.5) in form of configuration B is possible.

Theorem 4.3. *Consider the Riemann problem* (2.3), (2.5) *with the stiffened gas EOS* (2.2)*. If the 1- and 3-curves intersect in the point* (v^*, p^*) *with* $v^* > 0$*, then the following scenarios are possible.*

1. *If the point* (v^*, p^*) *lies between the left- and right-bounding 3-curves of Definition 4.2, then the configuration B is realizable, for all* $\mathbf{u}_L$ *on the 1- and for all* $\mathbf{u}_R$ *on the 3-curve. Moreover, the solution of this kind is unique, and the configuration C for the same Riemann problem is not realizable.*

2. *If the point* (v^*, p^*) *lies to the right of the right-bounding 3-curve, then there exists no solution to the Riemann problem* (2.3), (2.5) *in form of the configuration B.*

3. If $\mathrm{M}_L > 1$*, then the configuration A can be realizable.*

4. If $\mathrm{M}_R < -1$*, then the configuration D can be realizable.*

Proof. 1. For configuration B the states $\mathbf{u}_0$ must lie on the 1-curve. They are connected to the states $\mathbf{u}_1$ by 0-curves, such that these states $\mathbf{u}_1$ lie between the left- and right-bounding 3-curves, see Figs. 4, 5. Denote the projection of the set of all $\mathbf{u}_1$ to the (v, p)-plane by

$$S_1 = \{(v_1, p_1) \ : \ \mathbf{u}_1 = (A_1, \rho_1, v_1, p_1)^T\},$$

see Figs. 4, 5. The set S_1 is defined pointwise, with each point (v_1, p_1) belonging to different integral curves of (4.9). Therefore, S_1 lies on the differentiable integral surface, obtained by taking all integral curves of (4.9), such that $\mathbf{u}_1$ will are between the left- and right-bounding 3-curves.

Let us show that S_1 itself is a differentiable curve. All points $\mathbf{u}_1$ are given implicitly by the system (2.13), which can be rewritten as

$$\begin{aligned} F_1 &:= A_1\rho_1 v_1 - A_0\rho_0 v_0 = 0 \\ F_2 &:= \frac{p_1+\pi}{\rho_1^\gamma} - \frac{p_0+\pi}{\rho_0^\gamma} = 0 \\ F_3 &:= \frac{v_1^2}{2} + \frac{c_1^2}{\gamma-1} - \frac{v_0^2}{2} - \frac{c_0^2}{\gamma-1} = 0. \end{aligned} \tag{4.13}$$

The functions F_1, F_2, F_3 are differentiable with respect to all their arguments for $\rho > 0$ and the points $\mathbf{u}_0$ lie on the *smooth* 1-wave curve. We can calculate the Jacobian determinant of the system (4.13)

$$J = \left|\frac{\partial(F_1, F_2, F_3)}{\partial(\rho_1, v_1, p_1)}\right| = \frac{A_1}{\rho_1^\gamma}(c_1^2 - v_1^2).$$

Note that $J \neq 0$ unless $\mathbf{u}_1$ lies on the right-bounding 3-curve, which is excluded by the assumptions of the theorem. Then, by the implicit function theorem, S_1 will be a differentiable curve locally at every point (v_1, p_1).

From Lemma 4.1 it follows that the mapping $(v_0, p_0) \mapsto (v_1, p_1)$ is one-to-one. Since the points $\mathbf{u}_0$ lie on the strictly decreasing 1-wave curve, S_1 will be also strictly decreasing, see statement 3 of Lemma 4.1. Also, S_1 will approach the point on the 1-curve with $v = 0$ asymptotically, see statement 4 of Lemma 4.1. Since the 3-wave is strictly increasing, there exists a unique intersection point with S_1, see Figs. 4 and 5. This gives the solution to the Riemann problem (2.3), (2.5) in the framework of the configuration B.

Let us show that the configuration C for the same Riemann problem (2.3), (2.5) is impossible. Consider first the case $A_L < A_R$, see Fig. 6 (left). If the configuration C would be realizable, then the 0-wave would be next to the 3-wave, see Fig. 2. In the (v, p)-plane, it means that the possible states $\mathbf{u}_1$ must lie

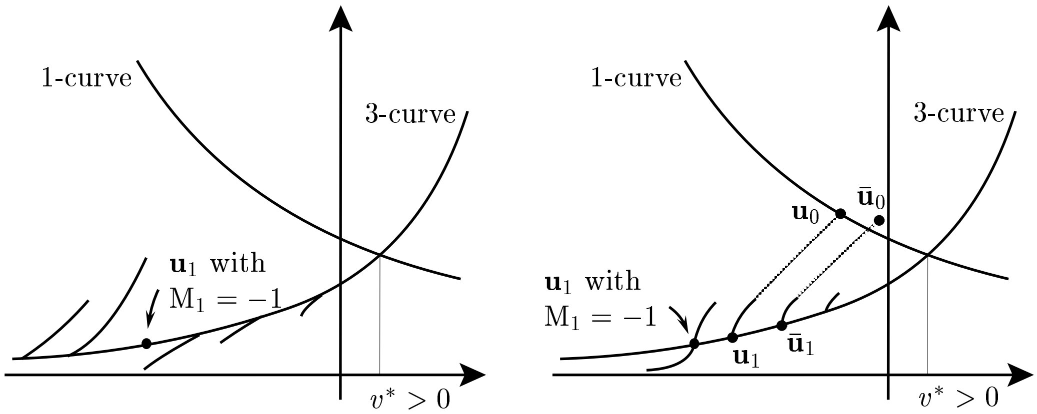

Fig. 6. Configuration C is impossible if the 1- and 3-wave curves intersect in a state with $v^* > 0$. Left: Case $A_L < A_R$. Right: Case $A_L > A_R$.

on the 3-curve, and the velocities in $\mathbf{u}_1$ would be negative. This follows from the fact that the eigenvalue v_0 for the 2-wave is negative, and $\operatorname{sign} v_0 = \operatorname{sign} v_1$. The states $\mathbf{u}_1$ with $\mathrm{M}_1 < -1$ are not admissible by the definition of configuration C. Indeed, then we would have $v_1 + c_1 < 0$, so that the 3-wave is either a sonic rarefaction (i.e. there is a sign change in the characteristic speed $v + c$), or a shock with negative speed. These both cases are excluded, see Fig. 2. Note that the 0-wave, starting from the $\mathbf{u}_1$ on the 3-wave, can never intersect the 1-wave, since for the case $A_L < A_R$ it points in the opposite direction, see Fig. 6 (left).

Now consider the case $A_L > A_R$, see Fig. 6 (right). The only possibility for the configuration C to be realizable would be if the state $\mathbf{u}_1$ on the 3-curve with $v_1 < 0$, $|\mathrm{M}_1| < 1$ were connected with the 1-curve via the 0-curve. Assume that this is true, i.e. there exists a state $\mathbf{u}_1$ with $v_1 < 0$, $|\mathrm{M}_1| < 1$, connected to $\mathbf{u}_0$ with $v_0 < 0$ on the 1-curve. Now let us move this state $\mathbf{u}_1$ towards the p-axis, so that it will become some state $\bar{\mathbf{u}}_1$, connected with $\bar{\mathbf{u}}_0$ by the 0-curve. As we move closer to the p-axis, the length L of the 0-curve, connecting $\bar{\mathbf{u}}_1$ with $\bar{\mathbf{u}}_0$, will remain positive by statement 3 of Lemma 4.1, since we have assumed that the 1- and 3-curves intersect in the point with $v^* > 0$, see Fig. 6 (right). This contradicts the statement 4 of Lemma 4.1, which states that L should shrink to zero. Thus, we have a unique way of connecting the 1- and 3-curves in form of configuration B, which is the intersection point of S_1 with the 3-curve.

2. This statement becomes obvious by considering Fig. 7. The 3-curve must lie to the right of the right-bounding 3-curve. For the case $A_L < A_R$, the state $\mathbf{u}_0$ on the 1-curve can be connected to a 3-curve only if $\mathrm{M}_0 > 1$, see Fig. 7 (left). This is impossible by the definition of configuration B. Indeed, in case $\mathrm{M}_L < 1$ we would have a sonic rarefaction in the solution of the Riemann problem. However, this is only possible if $A_L = A_R$, see [3]. In case $\mathrm{M}_L > 1$ we would have configuration A.

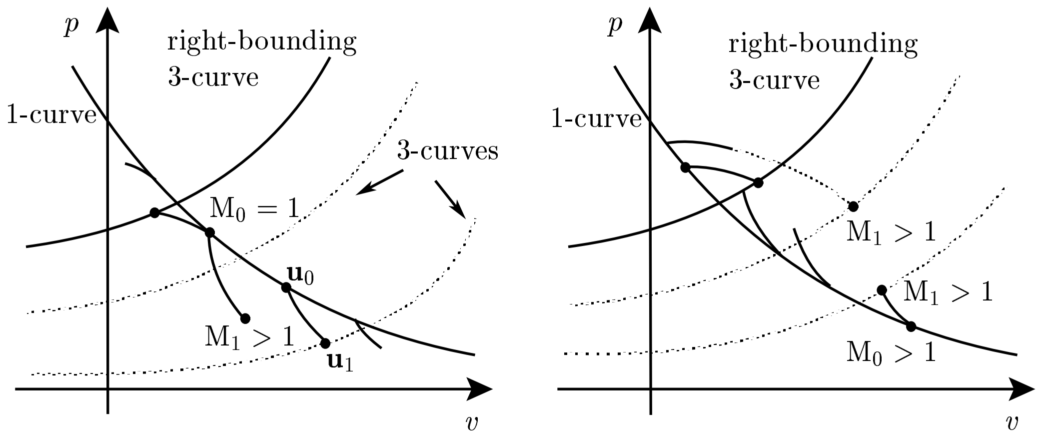

Fig. 7. Configuration B is impossible if the 1- and 3-wave curves intersect in a state with $v^* > 0$. Left: Case $A_L < A_R$. Right: Case $A_L > A_R$.

For the case $A_L > A_R$, the 0-curve can connect the 1- and 3-curves if either

(i) the 0-curve crosses the right-bounding 3-curve or

(ii) the state $\mathbf{u}_L$ is supersonic with positive velocity, $\mathrm{M}_L > 1$.

For the first case, the 0-curve would connect the subsonic state $\mathbf{u}_0$ with a supersonic one, which is impossible, see the properties of the 0-wave on page 9. For the second case we would have configuration A.

3. We prove this statement by giving several examples. Consider the following Riemann initial data

A_L	ρ_L	v_L	p_L	A_R	ρ_R	v_R	p_R
0.8	0.2069	3.991	0.07	0.8	0.1354	-3.1666	0.0833

. (4.14)

The wave curves for the Riemann problem (2.3), (4.14) are presented in Fig. 8 (top). Observe that for these initial data both configurations A and B are possible. The configuration A is realized when the left state $\mathbf{u}_L$ is connected first to the state $\bar{\mathbf{u}}_1$ with the 0-curve, and $\bar{\mathbf{u}}_1$ is then connected with $\bar{\mathbf{u}}^*$ via the 1-shock with speed $s = 0.948 > 0$. Note that if this speed would be negative, then the configuration A with these initial data would be not realizable, cf. Fig. 2. Since the intersection point of 1- and 3-curves lies between the left- and right-bounding waves (not shown in Fig. 8), the configuration B is also possible. For this configuration, the left state $\mathbf{u}_L$ is connected with $\mathbf{u}_0$ and the latter is connected with $\mathbf{u}_1$. The both wave configurations in (x, t)-plane are shown in Fig. 8 (bottom).

However, if we slightly modify the initial data (4.14), we can easily obtain a Riemann problem with a unique solution. For instance, for the Riemann prob-

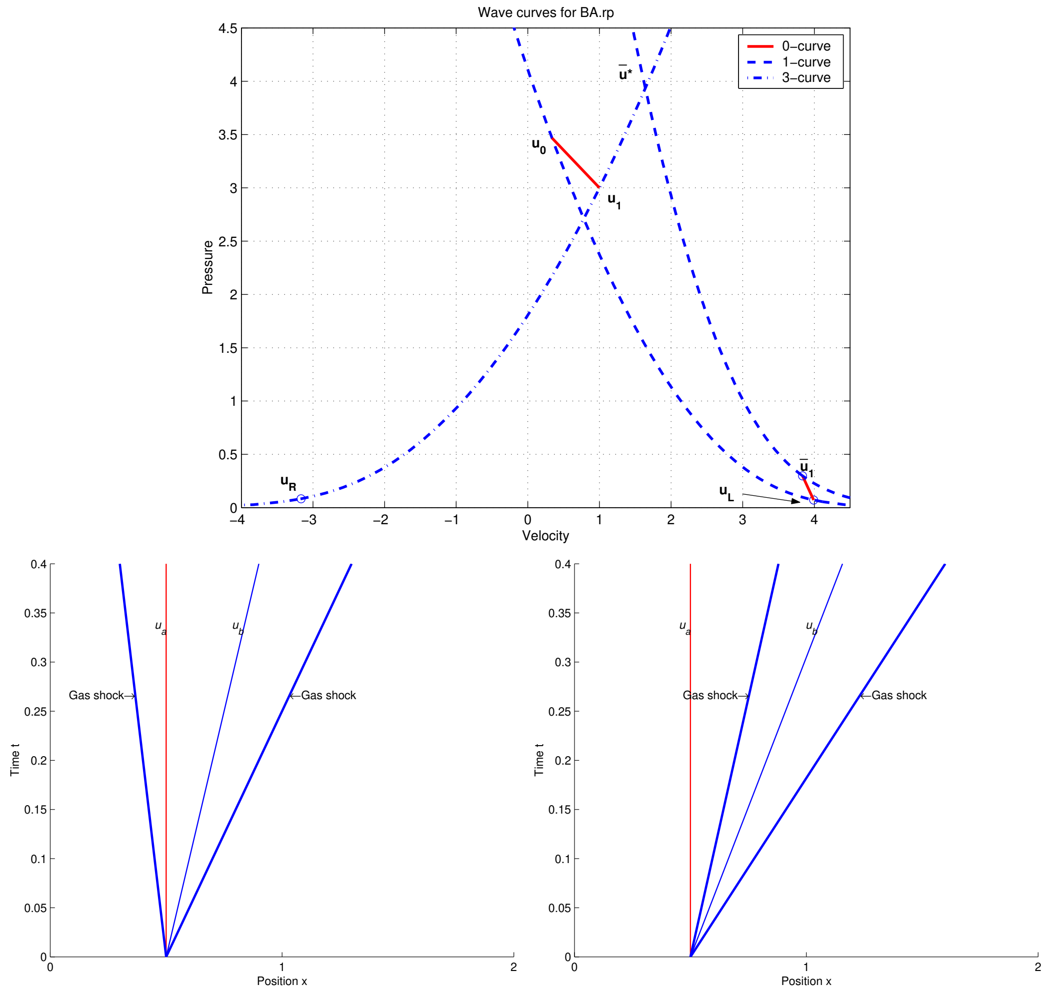

Fig. 8. Top: The wave curves for the Riemann problem (2.3), (4.14). Bottom: The corresponding wave configurations B and A in the (x, t)-plane.

lem (2.3) with the following initial data

A_L	ρ_L	v_L	p_L	A_R	ρ_R	v_R	p_R
0.8	0.2069	3.0	0.2	0.3	0.1354	-3.1666	0.0833

(4.15)

only the configuration B is possible. Indeed, consider the wave curves for this Riemann problem in Fig. 9. Again, the state $\mathbf{u}_L$ is first connected to the state $\bar{\mathbf{u}}_1$ with the 0-curve; from $\bar{\mathbf{u}}_1$, we draw the 1-curve till the intersection with the 3-curve, passing through $\mathbf{u}_R$. However, the corresponding wave will be a shock with negative speed $s = -0.198$. Therefore, the configuration A is now not possible. The configuration D is not possible for similar reasons. Since the 1- and 3-curves intersect between the corresponding left- and right-bounding 3-curves (not shown

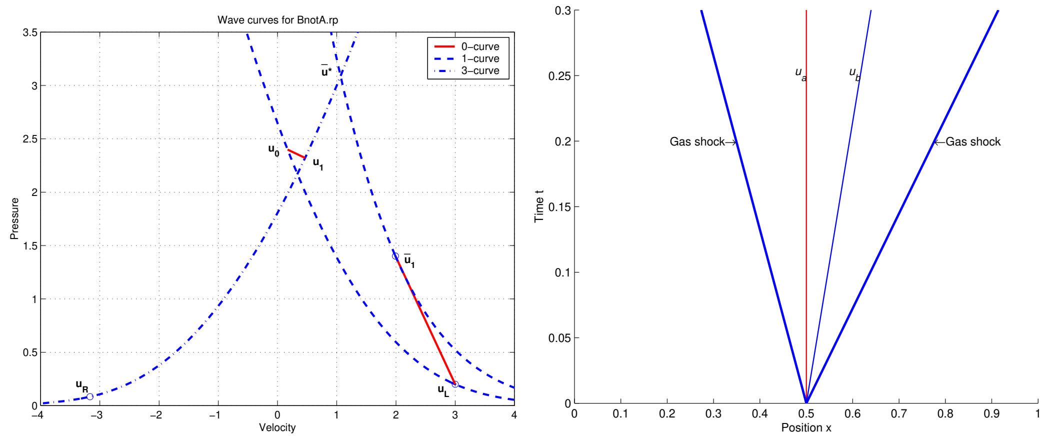

Fig. 9. The wave curves the for the Riemann problem (2.3), (4.15).

in Fig. 9), the configuration B is possible for the Riemann problem (2.3), (4.15). The waves in the (x, t)-plane for this Riemann problem are shown in Fig. 9 (right).

4. Consider the following Riemann initial data

A_L	ρ_L	v_L	p_L	A_R	ρ_R	v_R	p_R
0.3	0.2	3.3	1	0.8	0.2	-4	0.07

. (4.16)

Reasoning similar as above, we can show that the Riemann problem (2.3), (4.16) has a non-unique solution in form of either configuration B, or configuration D. The wave curves and the wave configurations are shown in Fig. 10.

□

For the configuration C, the results are completely analogous. The wave curves are presented in Figs. 11 and 12. Similarly to how it is done for the configuration B, one can introduce the left- and right-bounding curves.

Definition 4.4. *Consider the Riemann problem* (2.3), (2.5). *Let us call the 1-curve, crossing the 3-curve in the point with* $v = 0$ *the **right-bounding 1-curve**. Further,*

1. *If $A_L < A_R$, consider the state $\mathbf{u}_1$ on the 3-curve with $|\mathrm{M}_1| < 1$, connected with the state $\mathbf{u}_0$ with $\mathrm{M}_0 = -1$ by the 0-wave. Let us call the 1-curve, passing through this state $\mathbf{u}_0$, the **left-bounding 1-curve**, see Fig. 11.*

2. *If $A_L > A_R$, consider the state $\mathbf{u}_1$ on the 3-curve with $\mathrm{M}_1 = -1$, connected with the state $\mathbf{u}_0$ with $|\mathrm{M}_0| < 1$ by the 0-wave. Let us call the 1-curve, passing through $\mathbf{u}_0$ the **left-bounding 1-curve**, see Fig. 12.*

Analogously to Theorem 4.3 we have the following result.

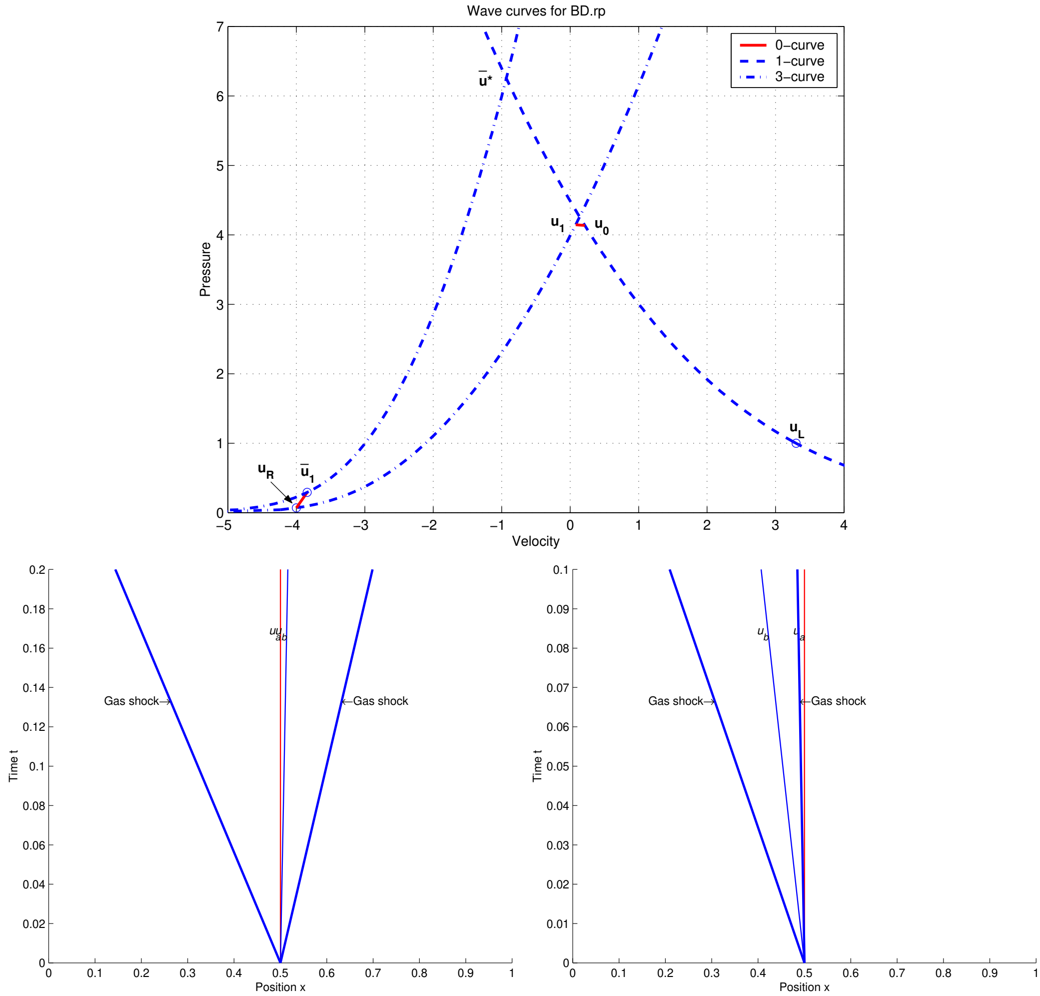

Fig. 10. Top: The wave curves for the Riemann problems (2.3), (4.16). Bottom: The corresponding wave configurations B and D in the (x,t)-plane.

Theorem 4.5. *Consider the Riemann problem* (2.3), (2.5) *with the stiffened gas EOS* (2.2). *If the 1- and 3-curves intersect in the point* (v^*, p^*) *with* $v^* < 0$, *then the following scenarios are possible.*

1. *If the point* (v^*, p^*) *lies between the left- and right-bounding 1-curves of Definition 4.4, then the configuration C is realizable, for all* $\mathbf{u}_L$ *on the 1- and all* $\mathbf{u}_R$ *on the 3-curve. Moreover, the solution of this kind is unique, and the configuration B for the same Riemann problem is not realizable.*

2. *If the point* (v^*, p^*) *lies to the left of the left-bounding 1-curve, then there exists no solution to the Riemann problem* (2.3), (2.5) *in form of the configuration C.*

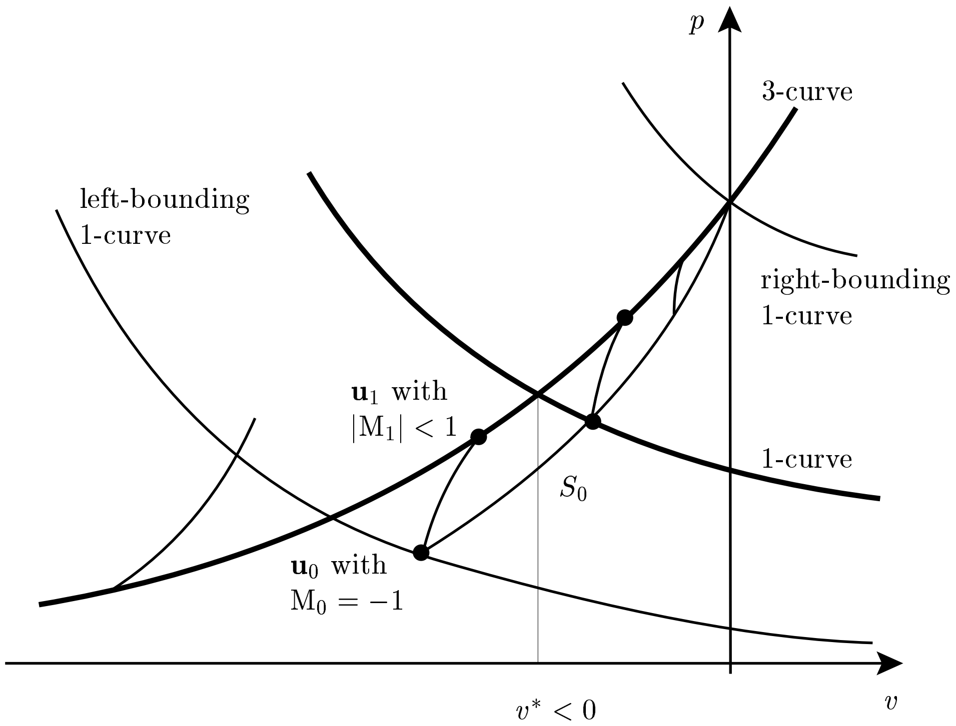

Fig. 11. The wave curves for the configuration C with $A_L < A_R$. If the point (v^*, p^*) lies between the left- and right-bounding 1-curves, there exists a unique solution in form of configuration C.

3. If $\mathrm{M}_L > 1$*, then the configuration A can be realizable.*

4. If $\mathrm{M}_R < -1$*, then the configuration D can be realizable.*

Proof. Analogous to the proof of Theorem 4.3. □

5 Which solution to take?

To understand the origin of the non-uniqueness of the Riemann solution for the Euler equations in a duct of variable cross-section, it is advantageous to consider analogous situations for other models. An immediate example is given by the usual Euler equations of gas dynamics. They are obtained as the inviscid approximation to, in general viscous, fluid flows. It is well known that this approximation leads to non-unique discontinuous solutions, and therefore to non-unique solutions for Riemann problems. One needs to use an additional criterion, entropy condition, in order to select the physically relevant solution. In fact, one possible way of obtaining an entropy condition is to add a viscous term to the Euler equations, i.e. to model the original viscous flow. Then the limit of solutions

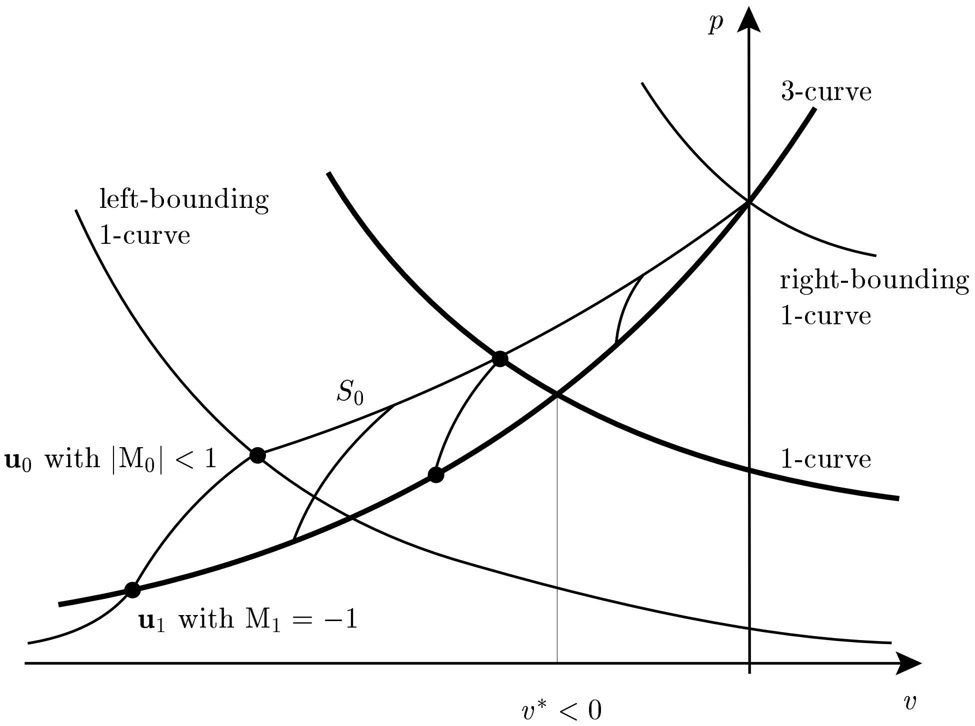

Fig. 12. The wave curves for the configuration C with $A_L > A_R$.

for vanishing viscosity will yield the physical entropy solution, see e.g. Godlewski and Raviart [15].

For the Euler equations in a duct of variable cross-section, the situation is somewhat analogous. In addition to neglecting viscosity, we have also neglected the multi- (two- or three-) dimensional effects. In this light it is not surprising that we got non-uniqueness of solutions to the Riemann problem. Roughly speaking, we have lost too much information on the truly multi-dimensional flow. However, one might hope to get a criterion for choosing the physically relevant solution by considering multi-dimensional effects, similarly to the limiting procedure for the usual Euler equations. One possible way would be to add some terms to the system of governing equations, which would model these effects. For example, these terms might be obtained using the statistical ensemble averaging techniques in the spirit of recent work of Abgrall and Saurel [1]. This could be an interesting topic of future research.

Here, we follow a more straight-forward approach: We compare the results of the quasi-one-dimensional Euler equations in a duct of variable cross-section with multi-dimensional computations of the usual Euler equations in a tube of corresponding geometry. To this end, we employ the popular software package CLAWPACK provided by LeVeque [8, 19]. It is efficient, robust, and simple to use.

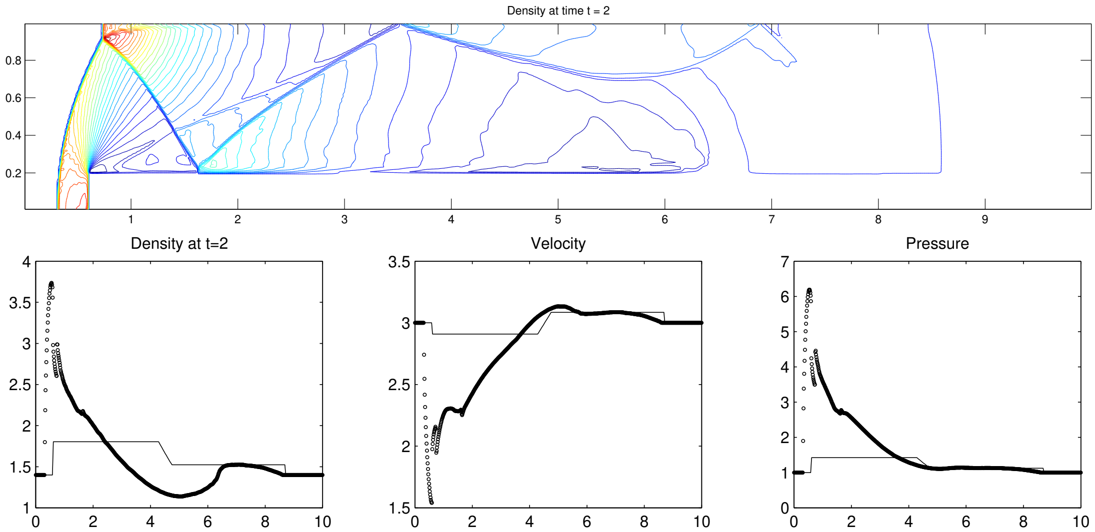

Fig. 13. Top: The density contours for the forward facing step problem. Bottom: The comparison of the averaged 2D solution (dots) with the 1D exact solution (line).

The basic building block is the user-defined Riemann solver, which is then incorporated in the so-called *wave propagation approach*. It splits the flux difference in the normal direction to the cell interface into two transverse flux differences. Then these differences are used to update the cell averages. Thus the algorithm reflects the fact that waves should propagate in a multi-dimensional manner. As a result, although CLAWPACK uses rectangular meshes, it is able to compute multi-dimensional flows correctly.

Before we start to judge which solution can be considered as physically relevant, we wish to assess the perfomance of the 1D model (2.3) on some well-known test cases. Remember that the Riemann problem for the quasi-one-dimensional flow in a duct of variable cross-section corresponds to the flow in a duct with a sudden jump in cross-section. There are a number of standard test cases, like the flow around a step (*forward-facing step*) or the diffraction of a shock wave at a corner (*backward-facing step*), which can be seen as the lower half of 2D flow in a duct with a sudden jump in cross-section. Therefore, we first compare the 2D CLAWPACK computations with the exact solution to the corresponding Riemann problem for the 1D model (2.3), and then do the same for the examples of Section 4. In the calculations below we have used CLAWPACK with a second order method, and Roe's Riemann solver, unless stated otherwise.

5.1 Forward-facing step

The forward-facing step is a test case, which is also often referred to as a *Mach 3 wind tunnel with a step*, see e.g. Woodward and Colella [26]. It is intensively used to compare different numerical schemes in 2D, see e.g. [26, 13]. The problem begins with uniform Mach 3 flow in a wind tunnel containing a step. The tunnel is 1 unit wide and the step of 0.2 units high is located 0.6 units to the right from the left-hand end of the tunnel. At the left(right) is an inflow(outflow) boundary condition. At the top and bottom reflecting boundary conditions are used. The unsteady solution consists of a bow shock, which is reflected several times from the upper and lower walls of the tunnel.

There are several difficulties concerning the numerical solution of this problem. The corner of the step is the center of a rarefaction fan and thus is a singular point of the flow. Due to this rarefaction, the pressures and densities may become negative in the computational cells just behind the corner. Also, the entropy tends to grow behind the corner and then is transported downstream, affecting the solution. To avoid this, one has to apply a special boundary condition at the corner, see [26]. Also, one may have numerical instabilities in the 2D strong almost stationary shocks in front of the corner and at the Mach stem at the upper wall, see again [26].

In our calculations with the Roe solver, we have obtained negative densities and pressures at the corner. To fix them, one can change to the HLLC solver [24, 7] there, which is positivity preserving in 1D. The 2D numerical results for 800×80 grid points are shown in Fig. 13 (top).

The corresponding initial data for the quasi-one-dimensional model (2.3) are

A_L	ρ_L	v_L	p_L	A_R	ρ_R	v_R	p_R
1	1.4	3	1	0.8	1.4	3	1

. (5.1)

The configuration of the Riemann problem (2.3), (5.1) and the wave curves for it are presented in Fig. 14.

The projections of the states $\mathbf{u}_L$ and $\mathbf{u}_R$ to the (v, p)-plane are represented by the same point, which is also their intersection point (v^*, p^*). Since $v^* = v_L = v_R = 3 > 0$, we are in conditions of Theorem 4.3. Since $\mathrm{M}_L = \mathrm{M}_R = 3$, the 3-curve lies to the right of the right-bounding 3-curve. Therefore, the configuration B in the solution of the Riemann problem (2.3), (5.1) is not realizable. The direct calculation shows that the configuration D is also impossible. The only possible solution in this case is configuration A, see Fig. 14. It consists of the 1-rarefaction, 2-contact, and 3-shock travelling to the right of the stationary 0-contact.

In Fig. 13 (bottom), the exact solution to the Riemann problem (2.3), (5.1) at time $t = 2$ is compared to the averaged 2D calculations. Observe that although the solutions differ considerably, the position of the 1D 3-shock gives relatively good approximation for the fastest wave in the averaged 2D solution.

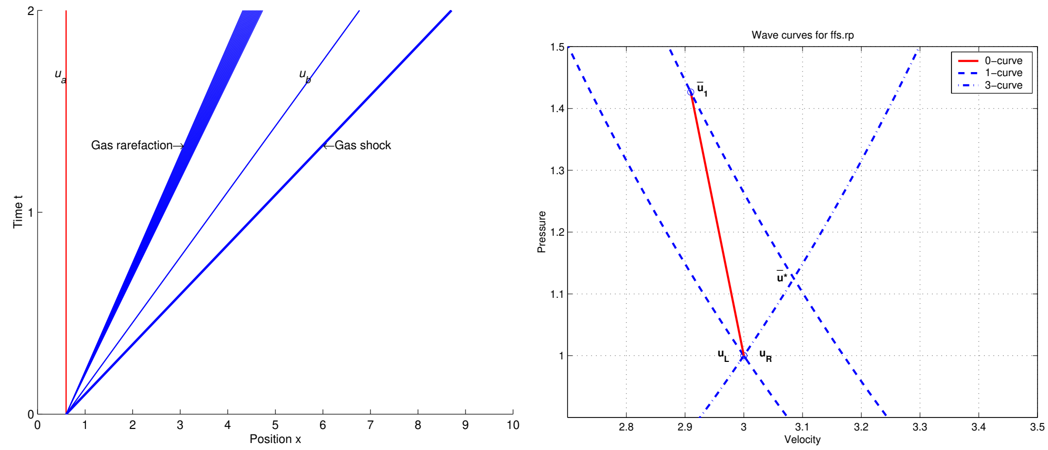

Fig. 14. The wave curves and the wave configuration for the 1D forward-facing step problem.

5.2 Backward-facing step

Here we consider two shock wave diffraction problems. The first one is described in Takayama and Inoue [23], and therefore will be referred to as *Takayama's test*. The shadowgraphs for the second problem were presented by Schardin, see Van Dyke [25]. This test will be referred to as *Schardin's test*.

Takayama's test The state behind the shock wave is given by $\rho = 1.862$, $u = 0.826$, $v = 0$, $p = 2.4583$, and in front of it by $\rho = p = 1$, $u = v = 0$. Thus, the shock moves with the speed $s = 1.7748$ and its Mach number is 1.5. The initial position of the shock can be taken at $x = 1.3$, and the computational domain is $[0, 2.6] \times [0, 2.6]$ without the south-west corner $[0, 1.3] \times [0, 1.3]$. The 2D solution is presented in Fig. 15 (left).

The initial data for the corresponding Riemann problem for the quasi-one-dimensional model (2.3) will be

A_L	ρ_L	v_L	p_L	A_R	ρ_R	v_R	p_R
1.3	1.862	0.826	2.4583	2.6	1	0	1

(5.2)

The wave curves are presented in Fig. 15.

Since the left and right states are connected by a single 3-shock, the projection of the intersection point of the 1- and 3-curves in the (v, p)-plane will coincide with the projection of $\mathbf{u}_L$, so the velocity there will be $v^* = v_L = 0.826 > 0$. We notice immediately that the 3-curve lies to the right of the right-bounding 3-curve, so that the configuration B is not realizable. Since the states $\mathbf{u}_L$, $\mathbf{u}_R$ are subsonic, the configurations A and D are not realizable as well. Therefore, the

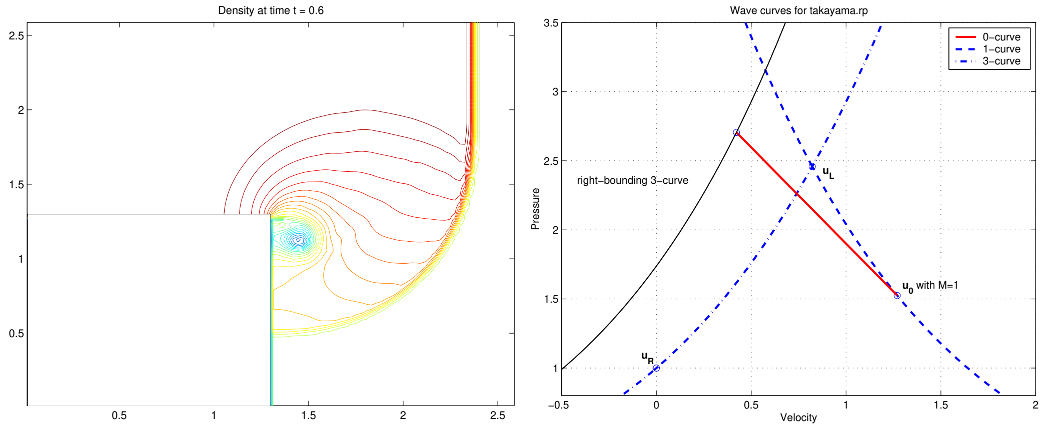

Fig. 15. The Takayama's test problem. Left: The 2D solution. Right: The wave curves for the corresponding Riemann problem (2.3), (5.2).

Riemann problem (2.3), (5.2) does not have a solution. At the same time, the 2D solution of the corresponding problem exists, see Fig. 15 (left).

Schardin's test Now the incident shock wave of Mach 1.3 diffracts over the north-west corner in the computational domain $([-6, 12] \times [0, 8]) \setminus ([-6, 1.5] \times [4, 8])$. The state behind the shock wave is given by $\rho = 2.122$, $u = 0.4423$, $v = 0$, $p = 1.805$, and in front of it by $\rho = 1.4$, $u = v = 0$, $p = 1$. The 2D solution is presented in Fig. 16 (top left).

The initial data for the corresponding Riemann problem for the quasi-one-dimensional model (2.3) will be

A_L	ρ_L	v_L	p_L	A_R	ρ_R	v_R	p_R
4	2.122	0.4423	1.805	8	1.4	0	1

. (5.3)

The wave curves are presented in Fig. 16 (top right).

Again, since the left and right states are connected by a single 3-shock, the projection of the intersection point of the 1- and 3-curves in the (v, p)-plane will coincide with the projection of $\mathbf{u}_L$, so the velocity there will be $v^* = v_L = 0.4423 > 0$. The 3-curve now lies between the left- and right-bounding 3-curves, so that the configuration B is realizable now. Since the states $\mathbf{u}_L$, $\mathbf{u}_R$ are subsonic, the configurations A and D are not realizable, so we have a unique solution to the 1D Riemann problem (2.3), (5.3).

In Fig. 16 (bottom) we present the comparison between the averaged 2D solution and the exact solution to the 1D Riemann problem (2.3), (5.3). We observe that the 1D model gives more or less correct wave speeds, slightly over-estimating the 3-shock speed. However, the 2D flow is too far away from being

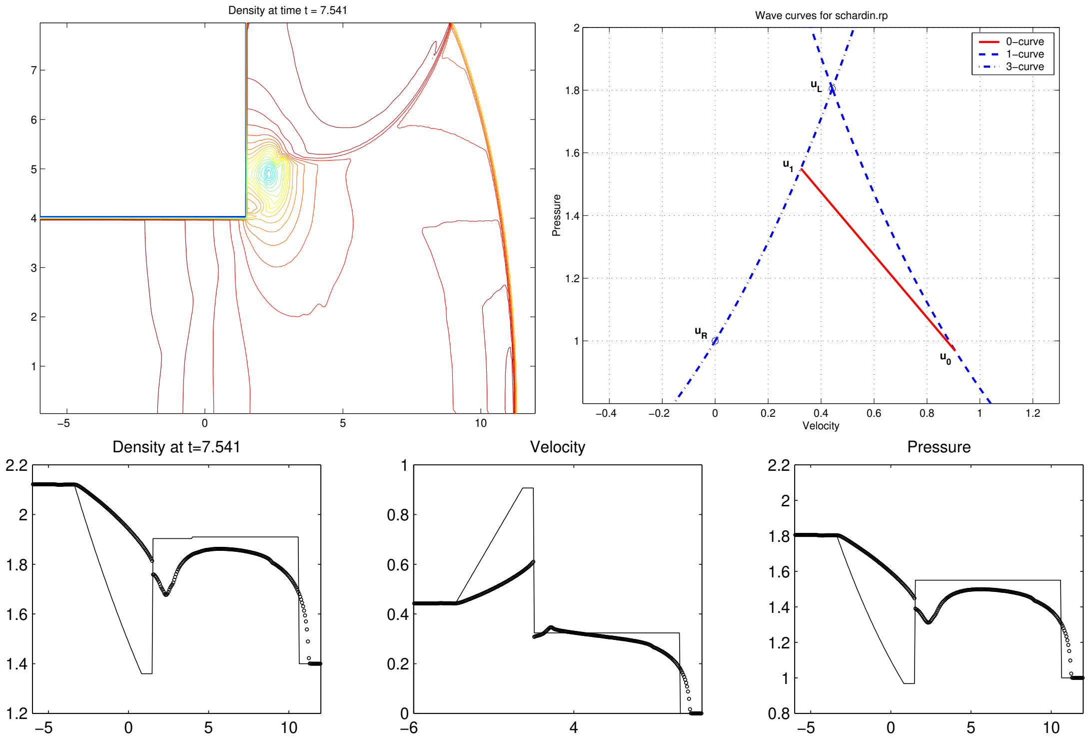

Fig. 16. The Schardin's test problem. Top left: The 2D solution. Top right: The 1D wave curves for the corresponding Riemann problem (2.3), (5.3). Bottom: The comparison of the averaged 2D solution (dots) with the 1D exact solution (line).

one-dimensional, so the 1D solution approximate it very poorly.

5.3 Diverse Riemann problems for the 1D model

Non-uniqueness between configurations A and B Consider the 1D Riemann problem (2.3), (4.14), which has already been studied in Section 4. This problem has a non-unique solution in form of either configuration A, or configuration B, see Fig. 8. With CLAWPACK, we solve the 2D analog of this 1D Riemann problem, i.e., the usual Euler equations in the corresponding 2D computational domain. The 2D solution on the 200×100 grid and the comparison of the averaged 2D solution with the exact solution to the 1D Riemann problem (2.3), (4.14) is shown in Fig. 17 (top). We see that the 1D model slightly over-estimates the 3-shock speed. Also, due to rich 2D motion in the left section of the domain, the 1D prediction of the position of 1-shock is quite approximate. The same can be said about the approximation of the flow near the jump in the cross-section. However, the numerical solution clearly picks up the configuration B in the 1D

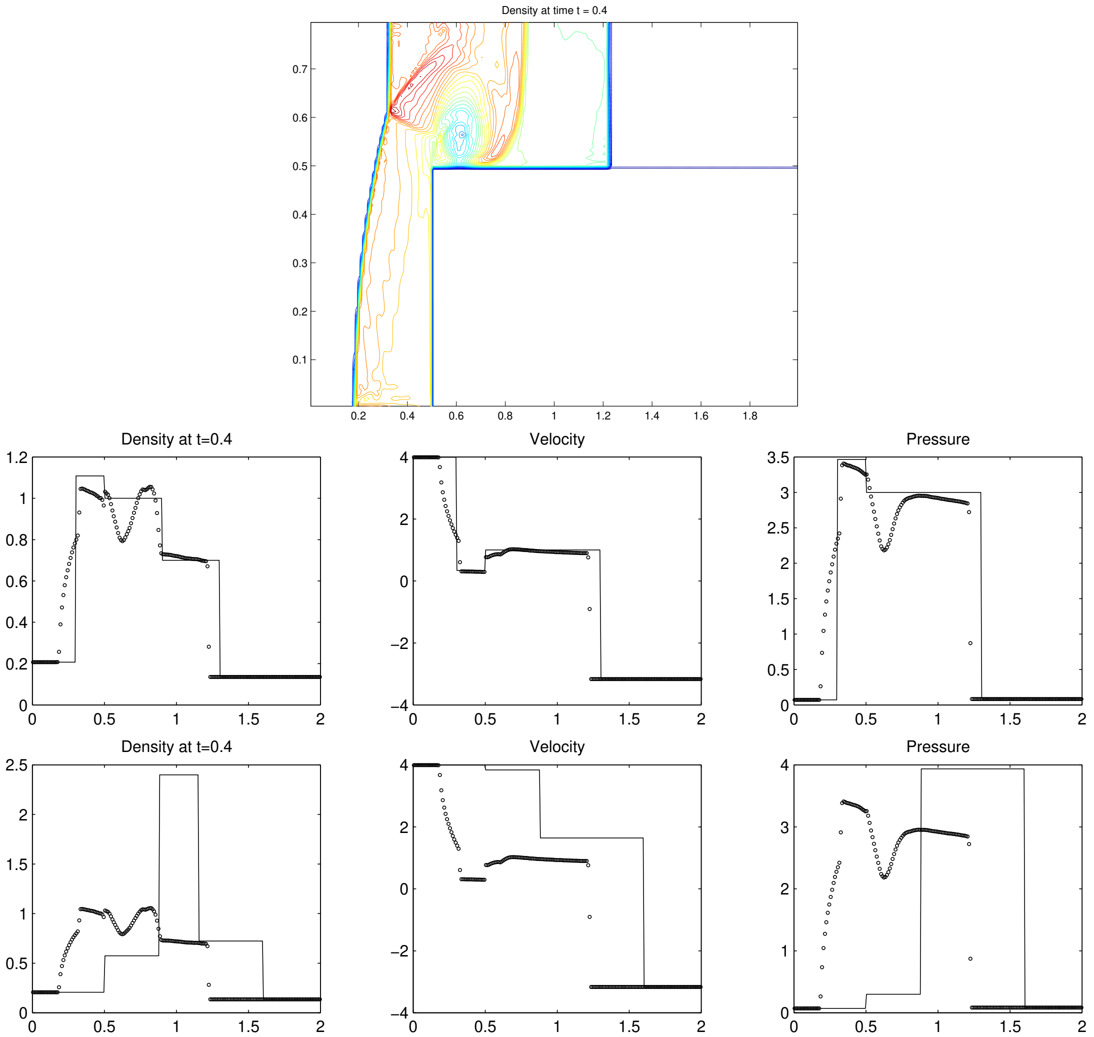

Fig. 17. Top: The density contours of the 2D solution to the Riemann problem (2.3), (4.14). Middle: The comparison of the averaged 2D solution (dots) with the 1D exact solution in form of configuration B (line). Bottom: The comparison of the averaged 2D solution (dots) with the 1D exact solution in form of configuration A (line).

solution of the Riemann problem (2.3), (4.14), see Fig. 17.

Unique solution in form of configuration B As we have established in Section 4, the Riemann problem (2.3), (4.15) has a unique solution in form of configuration B. The comparison of the averaged 2D solution on 100×100 grid with the exact solution to the 1D Riemann problem is shown in Fig. 18. Again, we observe that the shock speeds are slightly different, however the main features

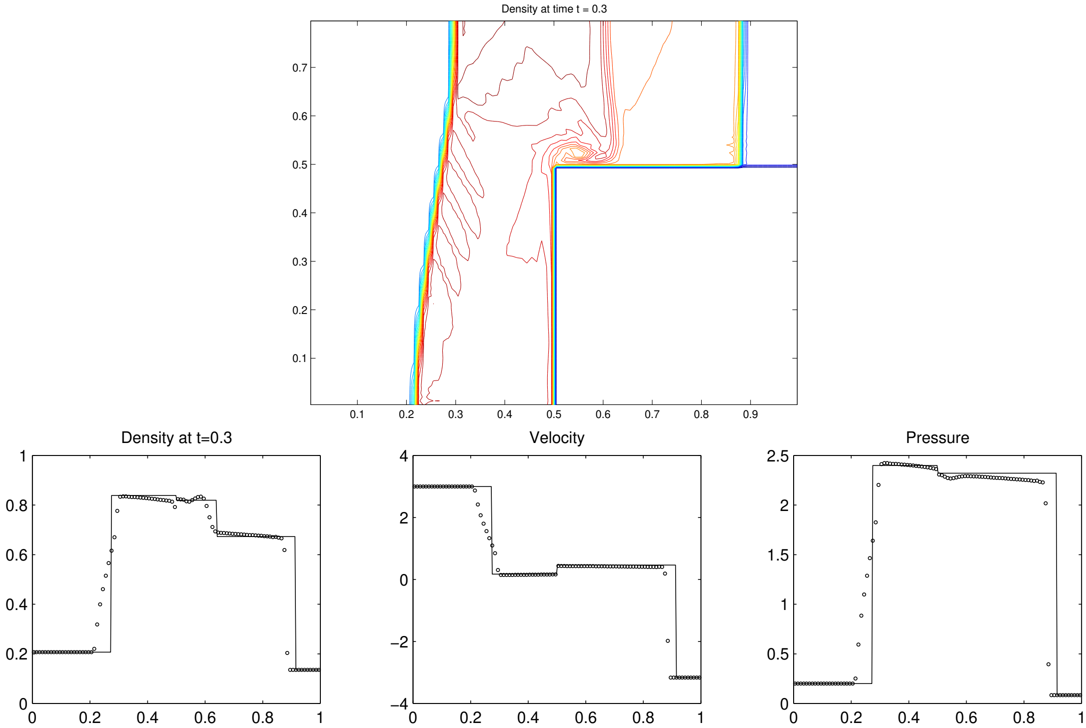

Fig. 18. Top: The density contours of the 2D solution to the Riemann problem (2.3), (4.15). Bottom: The comparison of the averaged 2D solution (dots) with the 1D exact solution (line).

of the 2D flow are correctly represented by the 1D model.

Non-uniqueness between configurations B and D The solution to the 1D Riemann problem (2.3), (4.16) is non-unique: It can be either configuration B, or configuration D. Again, we calculate the corresponding 2D problem and obtain the results, shown in Fig. 19. We see that the exact 1D solution for the configuration B fits perfectly to the averaged 2D solution. On the other hand, the 1D solution for configuration D has nothing in common with it; the left shock wave for the 1D solution even leaves the computational domain!

5.4 A criterion for realizable solutions

The preceeding computations show that for all configurations of Riemann problems the 1D solution can differ significantly from the 2D one, see e.g. the results for the forward facing step on Fig. 13 and for Schardin's test on Fig. 16. However, if the 1D solution to a Riemann problem is not unique, the 2D calculations clearly pick out one of them. In what follows, we will call the corresponding

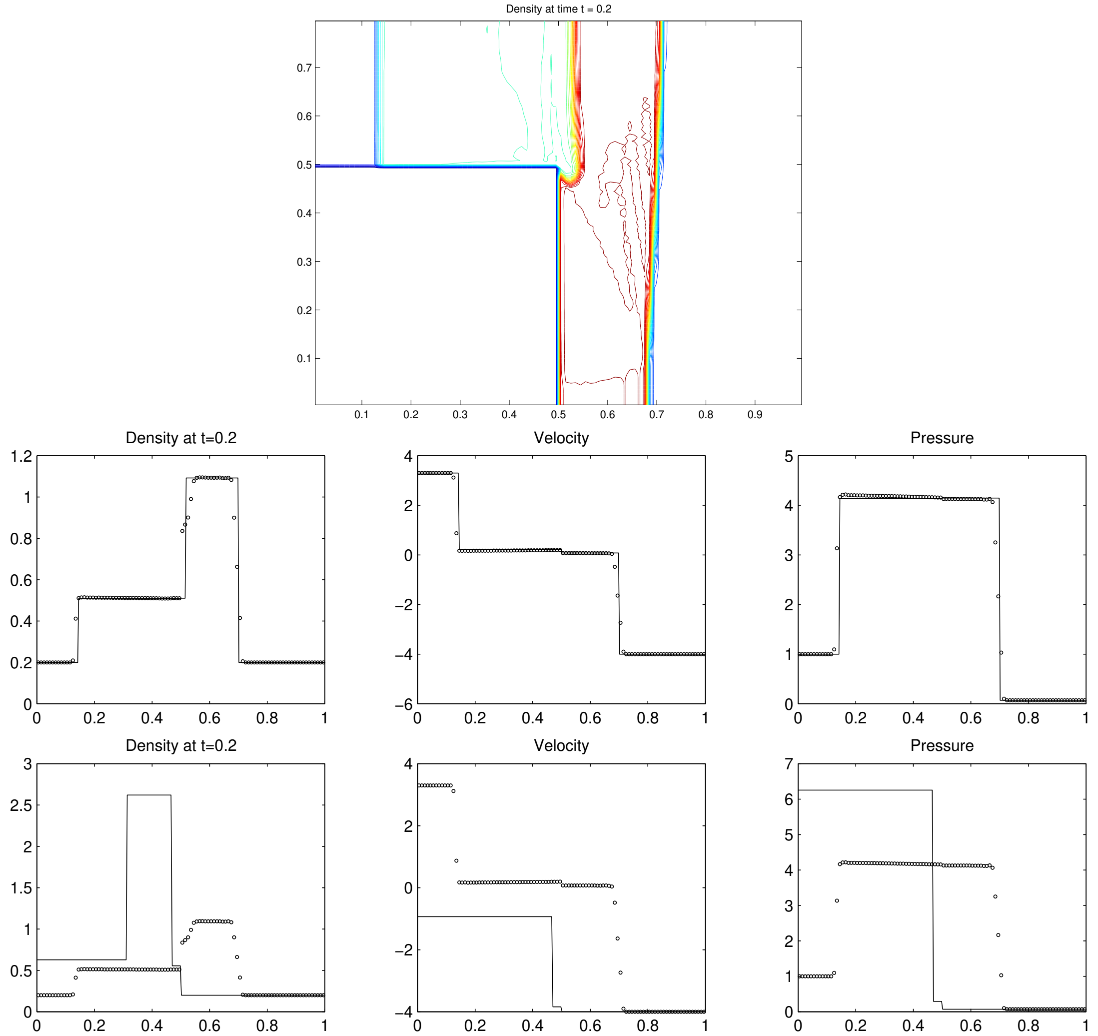

Fig. 19. Top: The density contours of the 2D solution to the Riemann problem (2.3), (4.16). Middle: The comparison of the averaged 2D solution (dots) with the 1D exact solution in form of configuration B (line). Bottom: The comparison of the averaged 2D solution (dots) with the 1D exact solution in form of configuration D (line).

1D Riemann solutions *physically relevant*. Let us investigate, what distinguishes these solutions from the physically non-relevant ones.

A classical way to exclude physically irrelevant solutions is to use a notion of entropy. However, one cannot use the entropy inequality used in the theory of conservation laws for the non-conservative system (2.3). In the particular case of the Riemann problem, one can use the approach of Section 3 to define it. Note also that *locally* each discontinuity in the solution to the Riemann problems is entropy-satisfying, i.e. the entropy increases across shocks. However, it does not help to rule out the physically irrelevant solutions. This suggests an idea of using a *global* entropy condition.

A condition of such kind was proposed by Dafermos [10, 11], who called it the *entropy rate admissibility criterion*. It states that not only should the entropy increase but it should be increasing at the maximum rate. The rigorous definition of this criterion can be applied for the conservation laws only. However, we can use the general idea for the non-conservative system (2.3) as well.

As a measure of the entropy increase rate, we use the jump in the isentrope $\eta = \frac{p+\pi}{\rho^\gamma}$ across shocks. These jumps are always positive. Then, our calculations show that physically relevant solutions, i.e. the ones picked out by 2D calculations, indeed have the maximal increase in entropy in comparison with the other solutions. This may be seen as an analogy of the entropy rate admissibility criterion of Dafermos [10].

Since the Euler equations in a duct can be formally obtained from the governing equations for the Baer–Nunziato model of two-phase flows [6], the solution to the Riemann problem for it will be in general also not unique. Therefore, the analysis of the Euler equations for a duct of variable cross-section and in particular the above criterion can help in investigating the properties of the governing equations for the Baer–Nunziato model.

6 The solution to the Riemann problem

Consider the Riemann problem for the system of the Euler equations in a duct of variable cross-section (2.3), (2.5), and let us look for an exact solution to it. Analogously to the case of the Baer–Nunziato model of two-phase flows [6], we can introduce the notion of the "inverse" solution to the Riemann problem, see [3]. Instead of starting with the end states $\mathbf{u}_L$, $\mathbf{u}_R$, and looking for the intermediate states in the solution of the Riemann problem, i.e. the "usual", or "direct" solution of the Riemann problem, we have fixed some intermediate state in the Riemann solution, prescribed the configuration of the Riemann problem, and looked for the end states $\mathbf{u}_L$, $\mathbf{u}_R$, which can be connected to this intermediate state by the prescribed waves, "inverse" solution.

Remember that the system (2.3) can be formally obtained from the governing equations for the Baer–Nunziato model of two-phase flows, see [3]. Therefore, we can use the procedure of the "inverse" solution which we have introduceed there, to construct exact solutions to the Riemann problems (2.3), (2.5). This procedure is implemented in the package CONSTRUCT [2]. It is designed for the Riemann problem for the Baer–Nunziato model of two-phase flows. For CONSTRUCTing exact solutions to the Euler equations in a duct of variable cross-section, one has to set the solid velocity equal to zero, and consider only the gas waves in the solution of the Riemann problem. The gas volume fraction then corresponds to the variable cross-section. Using CONSTRUCT, one can build numerical tests for assessing the accuracy of numerical methods of interest.

Now let us obtain the "direct" solution to the Riemann problem (2.3), (2.5). To do so, we remember that there are 4 possible configurations of this Riemann problem, see Fig. 2. Then, we solve the Riemann problem by examining if either of configurations A, B, C, or D is possible.

It is easy to check if the configurations A or D are realizable. Let us start with the configuration A. Since $\mathbf{u}_L$ is given, we can find $\mathbf{u}_1$ from the relations (2.13). To the right of the stationary contact, the system (2.3) reduces to the Euler equations. Now, we solve the Riemann problem for the Euler equations to the right of the stationary contact with the initial data $\mathbf{u}_1$ and $\mathbf{u}_R$. If the slowest wave speed in the solution of this Riemann problem is positive, then the configuration A is possible. Note that if the 1-wave is a rarefaction, and the last 1-characteristic speed is equal to zero, i.e. the 1-rarefaction touches the stationary contact from the right, then the parabolic degeneracy occurs, see Section 2. We do not consider this complicated case further.

We can treat the configuration D analogously. From $\mathbf{u}_R$, we can find $\mathbf{u}_0$. Next, we solve the Riemann problem to the left of the stationary contact with the initial data $\mathbf{u}_L$ and $\mathbf{u}_0$. Again, if the fastest wave speed is negative, then the configuration D is realizable. If the 3-wave is the rarefaction and it touches the stationary contact from the left, then the parabolic degeneracy occurs.

Checking for the configurations B and C is not so straightforward. Let us rewrite the relations (2.13) in the following way

$$\frac{p_0+\pi}{\rho_0^\gamma} = \frac{p_1+\pi}{\rho_1^\gamma} \tag{6.1}$$

$$A_0\rho_0 v_0 = A_1\rho_1 v_1 \tag{6.2}$$

$$\frac{\gamma(p_0+\pi)}{\rho_0(\gamma-1)}+\frac{v_0^2}{2} = \frac{\gamma(p_1+\pi)}{\rho_1(\gamma-1)}+\frac{v_1^2}{2}. \tag{6.3}$$

On the other hand,

$$v_0 = F_L(p_0) \tag{6.4}$$

$$v_1 = F_R(p_1), \tag{6.5}$$

where F_k, $k = L, R$ depends on wave type, i.e. if it is a shock or rarefaction,

$$F_k(p) = \begin{cases} v_k \pm (p-p_k)\left(\frac{A_k}{p+B_k}\right)^{\frac{1}{2}}, & \text{if } p > p_k \text{ (shock)} \\ v_k \pm \frac{2c_k}{\gamma-1}\left(\left(\frac{p+\pi}{p_k+\pi}\right)^{\frac{\gamma-1}{2\gamma}}-1\right), & \text{if } p \le p_k \text{ (rarefaction).} \end{cases} \tag{6.6}$$

Here the upper sign corresponds to the 3-wave, the lower to the 1-wave,

$$A_k = \frac{2}{\rho_k(\gamma+1)}, \qquad B_k = \frac{p_k(\gamma-1)}{\gamma+1}+\frac{2\gamma\pi}{\gamma+1}.$$

The equations (6.1)-(6.5) give the system of 5 equations for determining the 6 unknowns $\rho_0, v_0, p_0, \rho_1, v_1, p_1$. For the configurations B and C the closure is done in a different way. For the configuration B, we use

$$\rho_0 = R_L(p_0), \tag{6.7}$$

and for the configuration C

$$\rho_1 = R_R(p_1), \tag{6.8}$$

where

$$R_k(p) = \begin{cases} \rho_k \dfrac{\frac{p}{p_k} + \frac{\gamma-1}{\gamma+1} + \frac{2\gamma\pi}{p_k(\gamma+1)}}{\frac{p(\gamma-1)}{p_k(\gamma+1)} + 1 + \frac{2\gamma\pi}{p_k(\gamma+1)}}, & \text{if } p > p_k \text{ (shock)} \\ \rho_k \left(\dfrac{p+\pi}{p_k+\pi}\right)^{\frac{1}{\gamma}}, & \text{if } p \le p_k \text{ (rarefaction),} \end{cases}$$

and $k = L, R$. Putting all together, we have the nonlinear algebraic system for determining the states $\mathbf{u}_0$ and $\mathbf{u}_1$. We can rewrite it as

$$\mathcal{F}(\mathcal{W}) = 0, \tag{6.9}$$

where

$$\mathcal{W} = \begin{bmatrix} \rho_0 \\ v_0 \\ p_0 \\ \rho_1 \\ v_1 \\ p_1 \end{bmatrix}, \qquad \mathcal{F} = \begin{bmatrix} \frac{p_0+\pi}{\rho_0^\gamma} - \frac{p_1+\pi}{\rho_1^\gamma} \\ A_0\rho_0 v_0 - A_1\rho_1 v_1 \\ \frac{\gamma(p_0+\pi)}{\rho_0(\gamma-1)} + \frac{v_0^2}{2} - \frac{\gamma(p_1+\pi)}{\rho_1(\gamma-1)} - \frac{v_1^2}{2} \\ v_0 - F_L(p_0) \\ v_1 - F_R(p_1) \\ f_6 \end{bmatrix}, \tag{6.10}$$

and

$$f_6 = \begin{cases} \rho_0 - R_L(p_0) & \text{for configuration B} \\ \rho_1 - R_R(p_1) & \text{for configuration C.} \end{cases} \tag{6.11}$$

We solve the system (6.9) with the Newton method,

$$\mathcal{W}^{(n+1)} = \mathcal{W}^{(n)} - \mathcal{M}^{-1}(\mathcal{W}^{(n)}) \cdot \mathcal{W}^{(n)}, \tag{6.12}$$

where

$$\mathcal{M} = \begin{bmatrix} -\dfrac{\gamma(p_0+\pi)}{\rho_0^{\gamma+1}} & 0 & \dfrac{1}{\rho_0^\gamma} & \dfrac{\gamma(p_1+\pi)}{\rho_1^{\gamma+1}} & 0 & -\dfrac{1}{\rho_1^\gamma} \\ A_0 v_0 & A_0\rho_0 & 0 & -A_1 v_1 & -A_1\rho_1 & 0 \\ -\dfrac{\gamma(p_0+\pi)}{\rho_0^2(\gamma-1)} & v_0 & \dfrac{\gamma}{\rho_0(\gamma-1)} & \dfrac{\gamma(p_1+\pi)}{\rho_1^2(\gamma-1)} & -v_1 & \dfrac{\gamma}{\rho_1(\gamma-1)} \\ 0 & 1 & -F_L'(p_0) & 0 & 0 & 0 \\ 0 & 0 & 0 & 0 & 1 & -F_R'(p_1) \\ m_{61} & m_{62} & m_{63} & m_{64} & m_{65} & m_{66} \end{bmatrix},$$

and the last row of $\mathcal{M}$ depends on the configuration,

$$\mathcal{M}_6 = \begin{cases} \begin{bmatrix} 1 & 0 & -R'_L(p_0) & 0 & 0 & 0 \end{bmatrix} & \text{for configuration B} \\ \begin{bmatrix} 0 & 0 & 0 & 1 & 0 & -R'_R(p_1) \end{bmatrix} & \text{for configuration C} \end{cases} \tag{6.13}$$

It is well known that the convergence of the Newton method (6.12) depends strongly on the initial guess $\mathcal{W}^{(0)}$. Denote it by

$$\mathcal{W}^{(0)} = \left[\rho_0^{(0)}, v_0^{(0)}, p_0^{(0)}, \rho_1^{(0)}, v_1^{(0)}, p_1^{(0)}\right]^T, \tag{6.14}$$

so the starting guesses for the states on the both sides of the 0-wave will be $\mathbf{u}_i^{(0)} = \left[(\rho_i^{(0)}, v_i^{(0)}, p_i^{(0)}\right]^T$, $i = 0, 1$. From Section 4 we know which configuration (B or C) will be realizable for the particular Riemann problem, if it will be realizable at all, see Theorems 4.3, 4.5. From these theoremes it is clear that the correct states $\mathbf{u}_0$ and $\mathbf{u}_1$ on the both sides of the 0-wave lie close to the state $\mathbf{u}^*$, obtained by the intersection of the 1- and 3-curves in the (v, p)-plane. Therefore, we choose this state as the starting guess for both $\mathbf{u}_i^{(0)}$, $i = 0, 1$. With this choice, some tens of iterations in the Newton method (6.12) were needed in solving the Riemann problems of Sections 4 and 5.

There are several further options in implementing the Newton method for solving Riemann problems to (2.3). Since the solution across the stationary contact is not unique, cf. the analysis of [3], one could force $\mathbf{u}_0, \mathbf{u}_1$ to be the admissible states by solving the system of equations (2.13) for them at each Newton iteration. Also, it is possible that the densities and pressures become negative after some iteration. In this case, we simply set them to small positive values.

7 The Godunov-type method

Using the exact Riemann solver described above, one can develop a Godunov-type method for the non-conservative system (2.3) on its basis. Consider the system of the Euler equations in a duct (2.3), subject to the prescribed initial data $\mathbf{u}(x, 0)$. Assume we have an equally spaced grid, associated with the cell $I_j = [x_{j-1/2}, x_{j+1/2}]$, $x_{j+1/2} = j\Delta x$. At time $t^n = n\Delta t$, for each cell I_j, we define a cell average by

$$\mathbf{u}_j^n = \frac{1}{\Delta x}\int_{x_{j-1/2}}^{x_{j+1/2}} \mathbf{u}(x, t^n)\, dx. \tag{7.1}$$

Our key observation is that the cross-section A_j^n has a jump only across the cell boundary $x_{j+1/2}$ and is constant inside the cell I_j. Consequently, the non-conservative term $p\,\partial A/\partial x$ disappears in I_j and we are left with the *conservation law* there,

$$\mathbf{u}_t + \mathbf{f}(\mathbf{u})_x = 0, \tag{7.2}$$

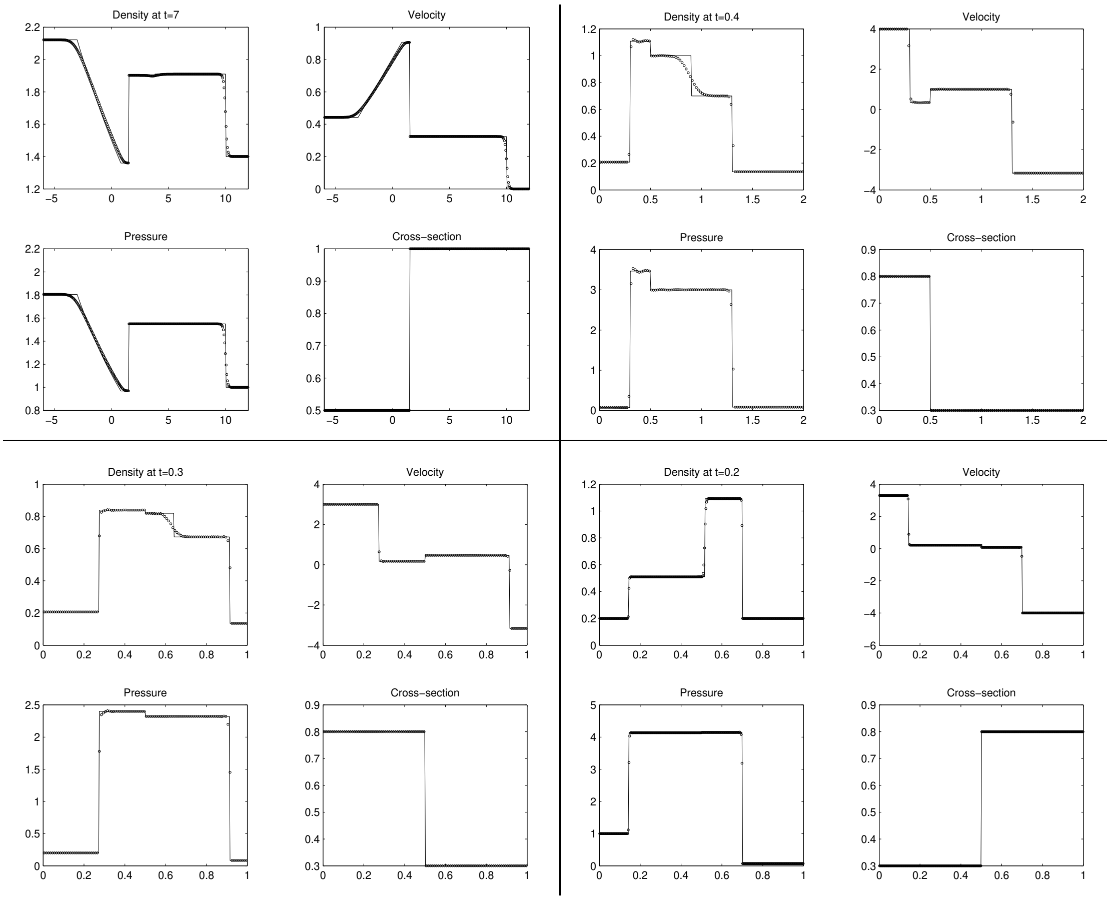

Fig. 20. Numerical results for the Godunov-type scheme (7.4). Top left: the Riemann problem (2.3), (5.3). Top right: the Riemann problem (2.3), (4.14). Bottom left: the Riemann problem (2.3), (4.15). Bottom right: the Riemann problem (2.3), (4.16).

where $\mathbf{u}$, $\mathbf{f}(\mathbf{u})$ are given by (2.4). Integrating (7.2) over $[x_{j-1/2}, x_{j+1/2}] \times [t^n, t^{n+1}]$ and using (7.1), we get

$$\mathbf{u}_j^{n+1} = \mathbf{u}_j^n - \frac{1}{\Delta x}\left[\int_{t^n}^{t^{n+1}} \mathbf{f}(\mathbf{u}(x_{j+1/2}, t))\, dt - \int_{t^n}^{t^{n+1}} \mathbf{f}(\mathbf{u}(x_{j-1/2}, t))\, dt\right]. \tag{7.3}$$

In the spirit of the classical Godunov method, we solve the Riemann problem at each cell boundary $x_{j+1/2}$ exactly, using the Newton method (6.12). Remember that the solution of this Riemann problem is self-similar, $\mathbf{u} = \text{const}$ along each ray $(x - x_{j+1/2})/t = \text{const}$. In general, $\mathbf{u}$ has a jump across the stationary contact $\lambda_0 = 0$. Denote the values to the left and to the right of it by $\mathbf{u}^-$ and $\mathbf{u}^+$, respectively. Using this in (7.3), the Godunov-type method reads

$$\mathbf{u}_j^{n+1} = \mathbf{u}_j^n - \frac{\Delta t}{\Delta x}\left[\mathbf{f}(\mathbf{u}_{j+1/2}^-) - \mathbf{f}(\mathbf{u}_{j-1/2}^+)\right]. \tag{7.4}$$

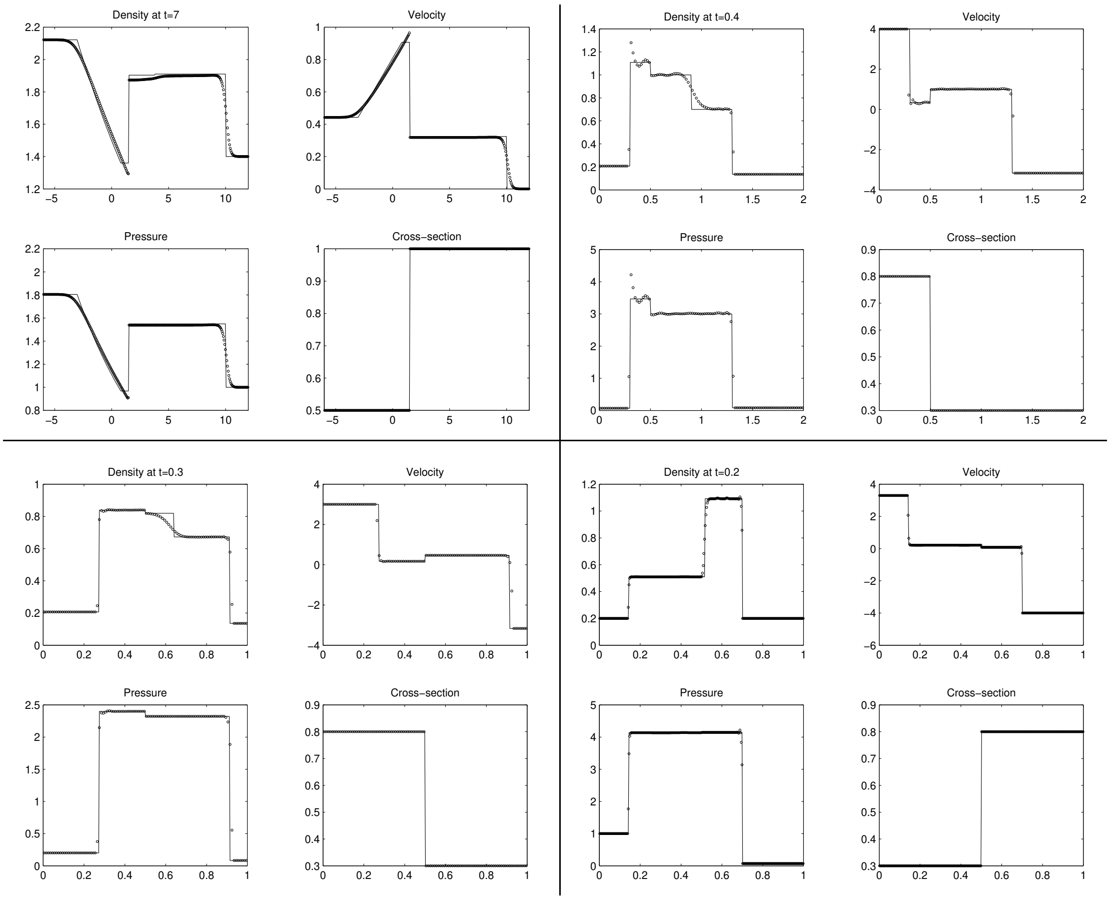

Fig. 21. Numerical results for the VFRoe scheme. Top left: the Riemann problem (2.3), (5.3). Top right: the Riemann problem (2.3), (4.14). Bottom left: the Riemann problem (2.3), (4.15). Bottom right: the Riemann problem (2.3), (4.16).

The above formula is valid as long as the CFL condition is fulfilled,

$$\frac{\Delta t}{\Delta x} \max |\lambda_i| \leq 1. \tag{7.5}$$

It guarantees that the $\mathbf{u}^{\pm}_{j+1/2}$ remain constant on each cell boundary $x_{j+1/2}$. The scheme (7.4) can be extended to second order via the MUSCL approach.

To test the Godunov-type method (7.4), we have solved several test cases of Sections 4 and 5. In Fig. 20, we present the first-order results, which were obtained on 300 mesh cells with a CFL number of 0.9. In general, the main features of the flow are correctly resolved. Note that the contact discontinuities are extensively smeared, which is typical for a first-order scheme. The second-order version of the scheme behaves significantly better for the contact discontinuities.

Initial data	VFRoe	Godunov
(5.3)	1.83	3.33
(4.14)	0.30	0.42
(4.15)	0.38	0.55
(4.16)	3.34	3.65

Table 1. User CPU time in sec as given by the UNIX command `time` on HP 9000 workstation.

Observe small oscillations in the vicinity of the 1-shock for the Riemann problem (2.3), (4.14) in Fig. 20. There are two possible reasons for such behaviour. The non-conservative system (2.3) is a particular case a resonant non-strictly hyperbolic system, which has been studied by a number of authors [16, 17, 20, 21, 14]. The properties of such systems can be investigated already in case of the 2×2 resonant nonlinear system, see Isaacson and Temple [17], Lin *et al.* [20, 21]. Their results show that when the wave speeds coincide, the total variation of the solution is not bounded by the total variation of the initial data. This can explain the oscillations for the 4×4 system (2.3) as well.

On the other hand, for the Riemann problem (2.3), (4.14) in Fig. 20, the 1-shock is slow, i.e. the ratio of the shock speed to the maximum wave speed is about 0.1. For the nonlinear systems of conservation laws, the problem of correct computation of slowly moving shocks with shock capturing schemes has been reported before, see e.g. [5, 18, 22]. The oscillations are generated already by first-order schemes, and become more pronounced in higher-order schemes due to their lower numerical dissipation. In course of time, these oscillations are transported downstream.

It is illuminating to compare the performance of the Godunov-type scheme (7.4) with the VFRoe method of [4]. We solve the problems, presented in Fig. 20, with VFRoe using the same run parameters, i.e. the first-order scheme, 300 mesh cells, and CFL = 0.9. The results are shown in Fig. 21. For some problems, the VFRoe scheme behaves quite reasonably, e.g. for the Riemann problems (2.3), (4.15) or (2.3), (4.16). However, we observe huge oscillations in the solution of the Schardin's test and the Riemann problem (2.3), (4.14). We have already witnessed such behaviour of the VFRoe scheme in [3] when discussing its perfomance for the Baer–Nunziato model of two-phase flows.

An obvious advantage of VFRoe over the Godunov-type scheme (7.4) is its speed. The CPU time needed for the solution of the problems, presented in Figs. 20 and 21, is given in Table 1. As we see, the VFRoe scheme is on average about 40% faster than the Godunov-type scheme (7.4). The reason for this is the presence of three iterative procedures in the Godunov-type scheme: (i) Exact solution to the Riemann problem for usual Euler equations, (ii) Exact solution behind the stationary contact, (iii) Newton's method (6.12). Note that for the particular case of a *Riemann problem*, i.e., the problems considered above, we employ Newton's method (6.12) only for the one local Riemann problem per time step, namely in the position of the initial discontinuity, the jump in cross-section is *stationary.* For more complicated problems, e.g. when the cross-section varies in the whole computational domain, we expect even bigger differences in speed for the VFRoe and Godunov-type methods.

References

[1] R. Abgrall and R. Saurel, Discrete equations for physical and numerical compressible multiphase mixtures, submitted to *J. Comp. Phys.* (2002). Available at
`hhttp://www.math.u-bordeaux.fr/abgrall/Articles/dipha.pdf`

[2] N. Andrianov, *CONSTRUCT: a collection of MATLAB routines for constructing the exact solution to the Riemann problem for the Baer-Nunziato model of two-phase flows.* Available at
`http://www.uni-magdeburg.de/andriano/CONSTRUCT`

[3] N. Andrianov and G. Warnecke, The Riemann problem for the Baer-Nunziato model of two-phase flows, submitted. Available at
`http://www.math.ntnu.no/conservation/2002/048.html`

[4] N. Andrianov, R. Saurel, and G. Warnecke, A simple method for compressible multiphase mixtures and interfaces, *Int. J. Numer. Meth. Fluids* **41**, 109-131, (2003).

[5] M. Arora and P. L. Roe, On postshock oscillations due to shock capturing schemes in unsteady flows, *J. Comput. Phys.* **130**, 25-40 (1997).

[6] M.R. Baer and J. W. Nunziato, A two-phase mixture theory for the deflagration-to-detonation transition (DDT) in reactive granular materials, *Int. J. of Multiphase Flows* **12**, 861-889 (1986).

[7] P. Batten, N. Clarke, C. Lambert, and D. M. Causon, On the choice of wavespeeds for the HLLC Riemann solver, *SIAM J. Sci. Comput.* **18**, 1553-1570, (1997).

[8] CLAWPACK software, available at
`http://www.amath.washington.edu/~claw/`

[9] R. Courant and K. O. Friedrichs, *Supersonic flow and shock waves,* Springer, New York, 1999.

[10] C. Dafermos, The entropy rate admissibility criterion for solutions of hyperbolic conservation laws, *J. Diff. Eqs.* **14**, 202-212 (1973).

[11] C. Dafermos, *Hyperbolic conservation laws in continuum physics*, Springer, Berlin, 2000.

[12] G. Dal Maso, P. G. LeFloch, and F. Murat, Definition and weak stability of nonconservative products, *J. Math. Pures Appl.* **74**, 483-548 (1995).

[13] R. Donat and A. Marquina, Capturing shock reflections: An improved flux formula, *J. Comp. Phys.* **125**, 45-58 (1996).

[14] P. Goatin and P. G. LeFloch, The Riemann problem for a class of resonant hyperbolic systems of balance laws, available at
`http://www.math.ntnu.no/conservation/2003/008.html`

[15] E. Godlewski and P.-A. Raviart, *Numerical approximation of hyperbolic systems of conservation laws,* Springer, New York, 1996.

[16] E. Isaacson and B. Temple, Nonlinear resonance in systems of conservation laws, *SIAM J. Appl. Math.* **52**, 1260-1278 (1992).

[17] E. Isaacson and B. Temple, Convergence of the 2×2 Godunov method for a general resonant nonlinear balance law, *SIAM J. Appl. Math.* **55**, 625-640 (1995).

[18] S. Karni and S. Čanić, Computations of slow moving shocks, *J. Comput. Phys.* **136**, 132-139 (1997).

[19] R. J. LeVeque, Wave propagation algorithms for multi-dimensional hyperbolic systems, *J. Comp. Phys.* **131**, 327-353 (1997).

[20] L. Lin, B. Temple, and J. Wang, A comparison of convergence rates for Godunov's method and Glimm's method in resonant nonlinear systems of conservation laws, *SIAM J. Num. Anal.* **32**, 824-840 (1995).

[21] L. Lin, B. Temple, and J. Wang, Supression of oscillations in Godunov's Method for a resonant non-strictly hyperbolic system, *SIAM J. Num. Anal.* **32**, 841-864 (1995).

[22] T. Roberts, the behaviour of flux difference splitting schemes near slowly moving shock waves, *J. Comput. Phys.* **90**, 141-160 (1990).

[23] K. Takayama and O. Inoue, Shock wave diffraction over a 90 degree sharp corner, *Shockwaves* **1**, 301-312 (1991).

[24] E. F. Toro, M. Spruce, and W. Spears, Restoration of the contact surface in the HLL Riemann solver, *Shock Waves* **4**, 25-34 (1994).

[25] M. Van Dyke, *An album of fluid motion*, Parabolic Press, 1982.

[26] P. Woodward and P. Colella, The numerical simulation of two-dimensional fluid with strong shocks, *J. Comput. Phys.* **54**, 115-173 (1984).

[27] M. J. Zucrow, J. D. Hoffman, *Gas dynamics*, vol. 2, John Wiley & Sons, 1977.